Rational Molecular Fragmentation Model As A Method For The Structural Analysis Of Large Drugs: A Case Study Concerning The Conformations Of Carvedilol In Terms Of Quantum Theoretical And Experimental NMR Spectroscopy

David R. P. Almeida

A dissertation submitted in conformity with the requirements of the Ph.D. degree

Institute of Pharmaceutical Chemistry
University of Szeged
Szeged, Hungary
2004

ABSTRACT

The pharmaceutical carvedilol acts as a non-selective beta (β_1/β_2) and selective alpha (α_1) adrenoceptor antagonist, cardioprotector, antioxidant, oxidative phosphorylation uncoupler, and amyloid-beta (Aβ) anti-fibrillar agent. Given its diverse pharmacodynamic profile, the resolution of carvedilol's highly populated conformations are a necessary prerequisite to divulging the basis of its molecular interactions. However, given carvedilol's sizeable conformational potential energy hypersurface (PEHS) - 11 torsional angles and 177 147 (3^{11}) conformational possibilities - this task requires a creative approach as traditional brute force multi-dimensional conformational analysis (MDCA) is impractical. Using carvedilol as a case study, a novel theoretical method entitled *rational molecular fragmentation* was developed for the structural and conformational study of complex drug molecules that minimizes computational and experimental resources. Rational molecular fragmentation was based on dividing carvedilol into simpler pharmacophore fragments (carbazole Fragment A, secondary amine Fragment B, and di-substituted benzene Fragment C) with manageable PEHSs but still relevant to the electronic structure of whole carvedilol.

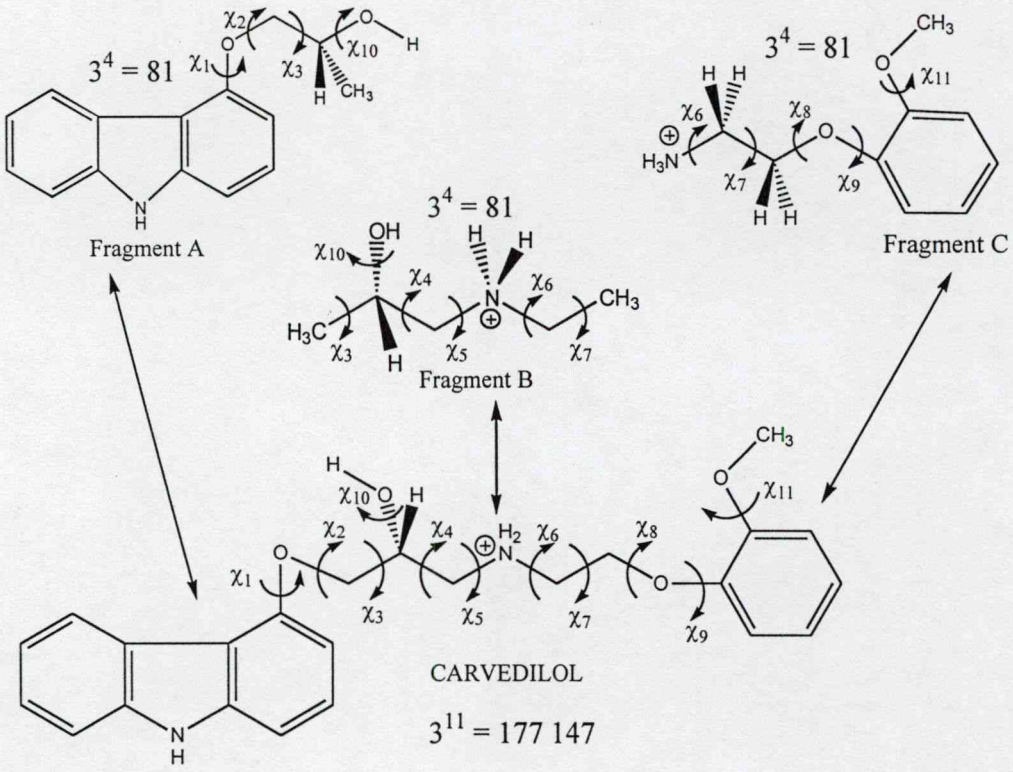

Each fragment was analyzed *via* gas phase Hartree-Fock [RHF/3-21G and RHF/6-31G(d)] and B3LYP/6-31G(d) density functional theory (DFT with the Becke 3LYP hybrid exchange-correlation functional) MDCA to disclose and assess dominant structures, structural motifs, conformational intricacies, stereochemical relationships (i.e., point chirality and axis chirality), multiple proton conformational basicity (particular to primary and secondary amines) parameters, and intramolecular attractive forces (IMAF) relevant to each fragment and to carvedilol. The dominant (low energy) fragment conformations, once optimized and evaluated, were used to hypothesize and predict a total of 240 carvedilol conformers which were initially optimized at the RHF/3-21G level of theory revealing 121 converged structures. An authentic set of nine converged low energy conformations were discovered and examined with DFT calculations in gas and solvent (DMSO and water). Independent NMR spectroscopy (in DMSO) was performed for further structural analysis and to verify the accuracy of this fragmentation method. Gas phase results show that seven of the nine conformers possess a novel tetra-centric spiro-type conformation composed of intramolecular six- and eight-membered rings. This structural motif is dictated by the positive nitrogen centre and by the inflexibility of the carbazole aromatic ring. DMSO and water DFT optimizations and NMR spectroscopy closely mirror each other indicating that carvedilol has a subtle energetic and structural solvent effect and a significant barrier to re-arrangement from gas phase to solvent exists. Given the harmony achieved between theoretical and experimental results, this study suggests the most populated states of carvedilol expected to dominate physical and biological samples and gives credence to the ability of methodically analyzing complex molecular systems by means of theoretical structure-activity fragmentation. Together, this will critically aid the molecular understating of carvedilol's pharmacodynamic mechanisms and structural underpinnings.

PREFACE

Modern computational techniques can be expressed within the three axes of molecular modeling: computer processing time, molecular system size (number of atoms), and degree of accuracy (c.f. **Figure I**); inherent in this description is that, since a finite amount of computer time exists, increasing a respective study along any one axis will force a trade-off in the other two[1]. Correspondingly, as a molecular system increases in size, its structural and conformational complexity increases exponentially as more degrees of freedom (e.g., torsional modes) are introduced (c.f. **Table I**; totals arrived at by means of multi dimensional conformation analysis [MDCA] where each torsional angle can assume *gauche* plus [*g*+], *anti* [*a*], or *gauche* minus [*g*-] orientations). Consequently, deciphering the dominant physical and biological conformations of a large molecular system becomes a daunting task.

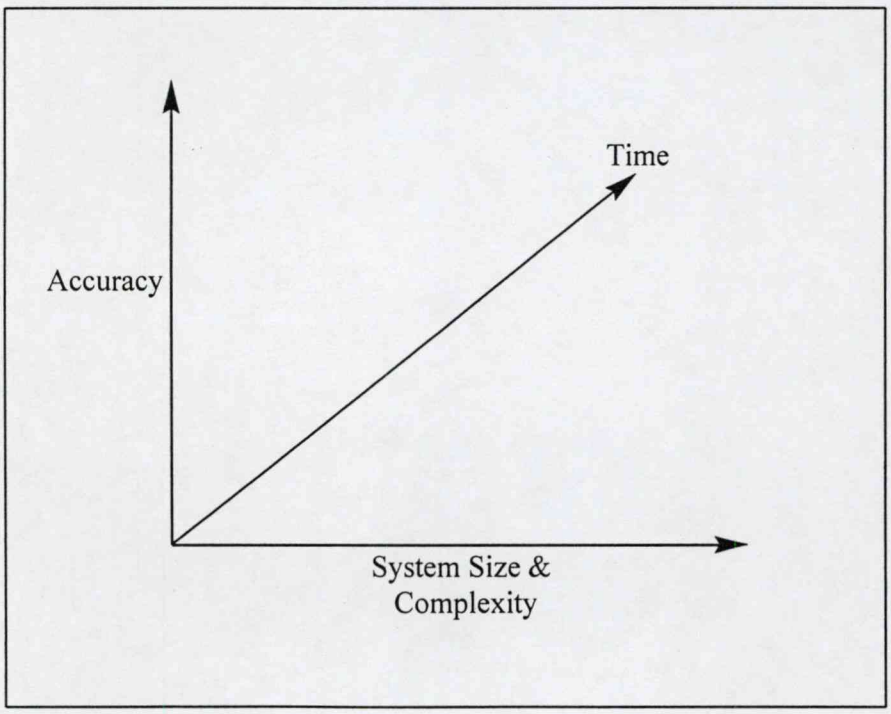

Figure I: The three axes of molecular modeling (adapted from reference **1**).

Table I: Number of torsional angles and corresponding conformational possibilities for a given molecular system. Totals for conformational possibilities arrived at by means of MDCA (each torsional angle can assume *g*+, *a*, or *g*- orientations).

Number of Torsional Angles	MDCA Conformational Possibilities
1	$3^1 = 3$
2	$3^2 = 9$
3	$3^3 = 27$
4	$3^4 = 81$
5	$3^5 = 243$
6	$3^6 = 729$
7	$3^7 = 2\ 187$
8	$3^8 = 6\ 561$
9	$3^9 = 19\ 683$
10	$3^{10} = 59\ 049$
11‡	$3^{11} = 177\ 147$
12	$3^{12} = 531\ 441$
13	$3^{13} = 1\ 594\ 323$
14	$3^{14} = 4\ 782\ 969$
15	$3^{15} = 14\ 348\ 907$

‡Number of torsional angles and conformational possibilities corresponding to carvedilol.

In the pharmaceutical sciences, drug molecules must not exceed a certain size, thus they may not contain more than 30 carbon, nitrogen, oxygen, or sulfur atoms, as well as the necessary number of hydrogens. Nonetheless, the problem of size and complexity is not bounded because the main conundrum for the pharmaceutical industry is the excessive number of molecules that need to be considered. **Figure II** shows the "Universe of Organic Molecules" in which molecules are arranged in such a way that similar structures are located close to each other[2]. Considering drug-sized molecules only, it may be estimated* that 10^{60} molecules are present in **Figure II**; "Corporate Libraries" (solid dots) and "Combinatorial Libraries" (heavily shaded areas) do not span, or do not adequately sample the "Universe of Organic Molecules". Furthermore, as more and more molecules are discovered and utilized, it becomes apparent that traditional experimental and theoretical First Principles methods will not able to reveal their active conformations within a suitable timeframe.

---

* Although the number of possible molecules is difficult to estimate accurately, simple considerations show that it must be very large. Consider growing a linear molecule, an atom at a time, and choosing a carbon, nitrogen, oxygen, or sulfur atom at each position. Some of these atoms can be double or triply bonded, but not all combinations of atoms are chemically stable, and some multiple bonds will only be possible in nonlinear structures (e.g., a C=O group). Assuming a very approximate average choice multiplicity of six, then 6^{30} or 2×10^{23} molecules could be grown containing 30 atoms. Now consider the ways of introducing branching or cyclization into the resulting structure. Closure of rings with three or more atoms involves selecting two atoms to form a bond and could be achieved on $30 \times {}^{28}/_{2}$ ways. Making a branched molecule could be achieved by choosing a point to cut the chain and a point in the first part of the chain to attach to the cut end of the second part of the chain (30^2 ways). Not all atoms can be joined in this way; however, this will be offset by the fact that when stereochemical considerations are introduced, the number of possibilities will be expanded. Based upon these considerations, approximately 10^{40} molecules with up to four rings and ten branch points could be produced from each linear chain, resulting in a very approximate estimate of 10^{63} molecules in total. Although this is a rough estimate, it seems likely that when all the different possible combinations of ring closure and branching are taken into account, the true number will be well in excess of 10^{60} and will rise steeply with increasing molecular weight[2].

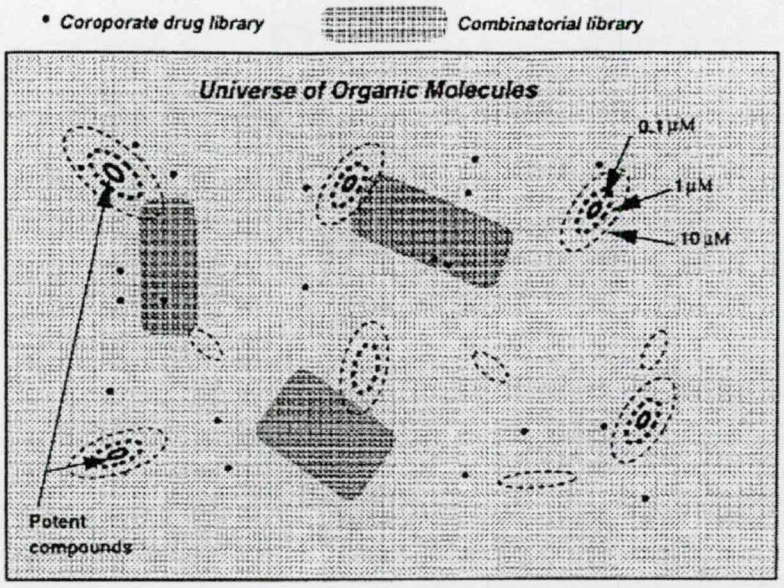

Figure II: A schematic illustration of the "Universe of Organic Molecules" and the scarcity of structural information in the drug discovery and design process (adapted from reference **2**). The concentration domains of active compounds are marked as 0.1, 1, and 10 µM.

As the drug design process propels itself at an ever-accelerating pace and the number of drug candidates, lead compounds, and approved agents increase - along with their size and complexity - it is clear we are at a crossroads for the structural and conformational study of drug molecules. Indeed, this problem is recognized:

> *"Clearly, studies must find more effective ways than brute force to sample the possible conformations. The challenge of sampling conformations is trying to ensure that we end up considering the most populated state, the global minimum... [Because] thermodynamics tells us that only low energy states are significantly occupied."*[1]

With regards to solutions, some principles are hinted at:

> *"The key to improved sampling will be combining an effective method for generating starting points with some amount of energy minimization. Diverse starting conformations will ensure a broad sampling of the potential energy surface and the conformations it represents. Energy minimizations will reduce the time spent considering high energy states by avoiding them during search for the local minima. Since generation of starting conformations and energy minimization use computer time, a balance must be struck that optimizes the search for the low energy structures."*[1]

Still, new methods are absent.

It quickly becomes evident that creative approaches are needed to remedy the above quandary. This dissertation presents a novel method, entitled *rational molecular fragmentation* that encompasses a computational viable framework and tool for the structural and conformational study of sizeable and complicated drug molecules. The cardiovascular pharmaceutical carvedilol will be used as a case study illustrating how this method is developed, drawn on, and delegated to reveal the structural and conformational intricacies of a particular molecular system. Given the lack of novel methods available, it is hoped that this model can be extrapolated for further molecular investigations.

References

1. E. Billings. Molecular Modeling and Drug Design. In Foye's Principles of Medicinal Chemistry, 5th ed.; Williams, D.A., Lemke, T.L., Eds.; Lippincott Williams & Wilkins: New York, 2002; pp 68-85.

2. R.S. Bohacek, C. McMartin, W.C. Guida; Med. Res. Rev. 16 (1996) 3.

TABLE OF CONTENTS

LIST OF TABLES

Table 14:
Water optimized values and energies for the converged conformers of the protonated *R*-carvedilol surface.

Table 15
NMR proton chemical shifts and assignments for carvedilol in DMSO (§ indicates NMR shifts cross-checked with reference **73**).

Table 16
Summary of conformation distribution for carvedilol and Fragments A, B, and C. Dominant torsional angle conformation for carvedilol and corresponding fragment conformation is bolded for ease of comparison. [‡]Conformation distribution is displayed as: number of conformations with respective torsional angle orientation/total number (i.e., nine) of conformations. [¥]Conformation distribution is displayed as: number of conformations with respective torsional angle orientation/total number of conformations (A = 4, B = 8, C = 6 conformations).

LIST OF FIGURES

Figure 10:
Molecular structures of the four low energy (defined as a conformer relative energy less than two Kcal•mol^{-1}) *R*-Fragment A conformers. Structures were fully optimized at the B3LYP/6-31G(d) level of theory (c.f. **Table 2** for optimized parameters).

Figure 11:
Optimized global minima (conformer *aaag*+) of the protonated Fragment B PEHS (left). All structures with an O11-nitrogen H_S/H_R proton H-bond displayed a similar structure characterized by an intramolecular five-membered ring. Newman projections along the C3-O11 bond (C3 front and O11 rear) display the *g*+, *anti*, and *g*- conformations of torsional angle χ_{10} at the stereocentre of Fragment B and carvedilol (right).

Figure 12:
Optimized global minima of the protonated Fragment C PEHS (*g*+*g*+*g*+*g*-) exhibits both a five- and eight-membered ring with a bifurcated H-bond (along with the global minima, all protonated conformers with relative energy less than two kcal•mol^{-1} has this structural feature). Conformer *g*+*aaa* has a moderate relative energy (5.95 kcal•mol^{-1}) and exhibits a five-membered ring while conformer *ag*+*aa* had the largest relative energy (22.45 kcal•mol^{-1}) of the protonated PEHS and possesses a fully extended conformation.

Figure 13:
Converged minima of the protonated Fragment C PEHS *g*+*ag*-*a* subset: *g*+*ag*-*a*^{A} (0.34 kcal•mol^{-1}), *g*+*ag*-*a*^{B} (1.75 kcal•mol^{-1}), and *g*+*ag*-*a*^{C} (1.78 kcal•mol^{-1}).

Figure 14:
Trends in $\Delta E_{vert}(S)$ and $\Delta E_{vert}(R)$ (left), $\Delta E_{opt}(S)$ and $\Delta E_{opt}(R)$ (middle), $\Delta\Delta E(S)$ and $\Delta\Delta E(R)$ (right) as compared to the conformer relative energy of converged Fragment B minima. Conformation Number labels are defined with superscripts in the χ_4 Protonated Conformation column of **Table 11**.

Figure 15:
Graphical representation of the conformer relative energies for all RHF/3-21G converged carvedilol structures.

Figure 16:
Schematic representation of the "tetra-centric" spiro-type conformational motif exhibited by most carvedilol low energy conformations. This structural motif consists of a six-membered ring (ring **a**) bonded to the carbazole centroid and an eight-membered ring (ring **b**) bonded to the substituted benzene. The intramolecular rings are formed by means of two short O···H-N H-bonds.

Figure 17:
Molecular structures (and relative energies) of conformers C-*R*-249 and C-*R*-251 optimized in the gas phase at the B3LYP/6-31G(d) level of theory (c.f. **Table 12** for optimized parameters).

Figure 18:
Graphical representation of the solvent effect of carvedilol. Gas, DMSO, and water phase relative energies are presented for all carvedilol structures optimized. Note that the DMSO and water relative energies extensively overlap each other.

Figure 19:
Molecular structure of the DMSO and water solvent global minima, conformer C-*R*-250, optimized at B3LYP/6-31G(d).**Figure 3:**

Figure 20:
Graphical representation of the relationship between J-coupling and NOE intensity for protons H45 (left) and H44 (right) to stereocentre proton H43.

Figure 21:
Newman projection of the *g*+ orientation for torsional angle χ_4 of carvedilol found in all gas phase, DMSO, and water optimized structures (c.f. **Tables 12, 13, and 14**).

Figure 22:
Diagrammatical representation of the rational molecular fragmentation method applied for the structural analysis of complex molecular systems. Note that, as shown for the carvedilol case study, conformations, as well as other structural parameters (stereochemistry, basicity, H-bonding, etc.), may be analyzed, predicted, optimized, resolved, and extrapolated with this approach to structural analysis.

ACKNOWLEDGEMENTS

The author wishes to acknowledge the encouragement and moral support of Professor Ferenc Fülöp. The author is also grateful to Mr. Jose Almeida, Ms. M. Fernanda P. Almeida, Ms. Donna M. Gasparro, Mr. Luca F. Pisterzi, Dr. Tamàs A. Martinek, and Professor Imre G. Csizmadia for their inspiration and guidance during this research as well as during the preparation of this dissertation.

PUBLISHED OR ACCEPTED OR SUBMITTED PAPERS

1. **David R. P. Almeida**, Luca F. Pisterzi, Gregory A. Chass, Ladislaus L. Torday, Andras Varro, Julius Gy. Papp, and Imre G. Csizmadia. A density functional molecular study on the full conformational space of the *S*-4-(2-hydroxy propoxy)carbazol fragment of carvedilol (1-(9H-Carbazol-4-yloxy)-3-[2-(2-methoxy-phenoxy)ethylamino]-2-propanol) in vacuum and in different solvent media, J. Phys. Chem. A, 106 (**2002**), 10423-10436.

   IF: **2.765**

2. **David R. P. Almeida**, Donna M. Gasparro, Luca F. Pisterzi, Ladislaus L. Torday, Andras Varro, Julius Gy. Papp, and Botond Penke. Gas phase conformational basicity of carvedilol Fragment B, 2(S)-1-(ethylamonium)propane-2-ol: An ab initio study on a protonophoretic of oxidative phosphorylation uncoupling, J. Mol. Str. (THEOCHEM), 631 (**2003**), 251-270.

   IF: **1.014**[§]

3. **David R. P. Almeida**, Donna M. Gasparro, Luca F. Pisterzi, Ladislaus L. Torday, Andras Varro, Julius Gy. Papp, Botond Penke, and Imre G. Csizmadia. Molecular study on the enantiomeric relationships of carvedilol Fragment A, 4-(2-hydroxypropoxy)carbazol, along with selected analogues, J. Phys. Chem. A, 107 (**2003**), 5594-5610.

   IF: **2.765**[†]

4. **David R. P. Almeida**, Donna M. Gasparro, Luca F. Pisterzi, Jason R. Juhasz, Ferenc Fülöp, and Imre G. Csizmadia. Conformational-dependent basicity of carvedilol Fragment C: An ab initio study on the primary amine, aminoethoxy-2-methoxy-benzene, J. Mol. Str. (THEOCHEM), 666-667 (**2003**), 557-580.

   IF: **1.014**[§]

5. **David R. P. Almeida**, Donna M. Gasparro, Luca F. Pisterzi, Jason R. Juhasz, Ferenc Fülöp, and Imre G. Csizmadia. Predicting the conformations of carvedilol based on its pharmacophore fragments: A gas phase and solvation ab initio and density functional study, J. Mol. Str. (THEOCHEM), 666-667 (**2003**), 537-545.

   IF: **1.014**[§]

6. **David R. P. Almeida**, Donna M. Gasparro, Ferenc Fülöp, and Imre G. Csizmadia. Pharmacophore fragment-based prediction and gas phase ab initio optimization of carvedilol conformations, J. Phys. Chem. A, (**2004**), in press.

   IF: **2.765**[†]

7. **David R. P. Almeida**, Donna M. Gasparro, Tamas A. Martinek, Ferenc Fülöp, and Imre G. Csizmadia. Resolution of carvedilol's conformational surface via gas and solvent phase density functional theory optimizations and NMR spectroscopy, J. Phys. Chem. A, submitted for publication (**2004**).

   IF: **2.765**[†]

PUBLISHED OR ACCEPTED PAPERS: **6**

Cumulative IF: **11.337**

SUBMITTED PAPERS: **1**

First Author in: **7**

[§] J. Mol. Str. (THEOCHEM) 2002 impact factor used because 2003 impact factor value not available at the time of printing this dissertation.

[†] J. Phys. Chem. A 2002 impact factor used because 2003 and 2004 impact factor values not available at the time of printing this dissertation.

1. Introduction

1.1 Biological & Pharmacodynamic Review of Carvedilol

The cardiovascular pharmaceutical carvedilol, 1-[carbazolyl-(4)-oxy]-3-[(2-methoxyphenoxyethyl)amino]-2-propanol ($C_{24}H_{26}N_2O_4$), is a hydrophobic aryloxypropanolamine multiple-action neurohormonal antagonist (c.f. **Figure 1**)[1]. Carvedilol is used in the treatment of mild-to-moderate essential hypertension, stable angina pectoris, ischemic heart disease (IHD), and mild-to-moderate chronic congestive heart failure (CHF)[2-5]. The major molecular targets of carvedilol are: membrane adrenoceptors (β_1/β_2 and α_1)[1], reactive oxygen species (ROS)[6-10], mitochondria oxidative phosphorylation[11], ion channels (K^+ and Ca^{2+})[12], neurohumoral factors (nitric oxides, endothelins, natriuretic peptides)[13,14], and amyloid-beta (Aβ) peptide(s)[15]. Carvedilol's therapeutic potential proved to be so remarkable that the United States Data and Safety Monitoring Board (US DSMB) stopped, for ethical reasons, carvedilol's clinical investigation before completion due to greatly lowered mortality rates[16,17].

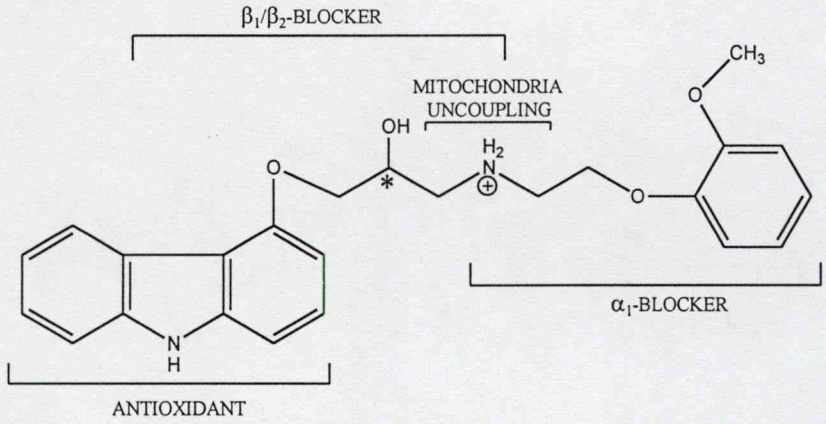

Figure 1: Molecular structure and pharmacophore structure-activity of N-protonated carvedilol (* indicates stereocentre).

As a non-selective β-blocker, carvedilol antagonizes noradrenaline at β_1- (heart muscle, kidney) and β_2- (certain blood vessels, smooth muscle of some organs) adrenoceptors reducing total cardiac work while maintaining stroke volume and cardiac output[1,18-20]. Antagonist action at α_1-adrenergic receptors (found in most sympathetic target tissues) causes vasodilation at peripheral resistance vessels, which decreases pre-load and after-load, thereby further reducing cardiac work and

wall tensions[21]. Carvedilol's reduction in blood pressure is primarily due to the concomitant antagonist action at α_1-adrenoceptors which causes peripheral vasodilation and the β_1/β_2-antagonism that prevents reflex tachycardia[22,23].

Carvedilol, along with three of its metabolites (c.f. **Figure 2**), have novel antioxidant properties, due to the carbazole moiety, not found in other β-blockers[24]. The aromatic carbazole centroid has a low redox potential which gives carvedilol and its metabolites a powerful tendency to donate electrons more readily and "scavenge" the activities of oxygen-containing free radicals (electrons move spontaneously towards oxidant species with more positive redox potentials) such as: oxygen superoxide ($O_2^{\bullet -}$), hydrogen peroxide (H_2O_2), hydroxyl radical (•OH), and peroxynitrite ($ONOO^{\bullet -}$)[25]. Carvedilol has also been shown to inhibit lipid peroxidation due to its capacity to both scavenge ROS and sequester ferric ions (Fe^{3+}) in lipid membranes[26-28].

Carvedilol protects endothelial, neuronal, and vascular smooth muscle from oxidative stress and inhibits ROS-mediated oxidation of low-density lipoprotein (LDL) particles[23]. The antioxidant activity of carvedilol is approximately ten times greater than α-tocopherol (vitamin E)[23,29] and carvedilol's metabolite, 1-hydroxyl carvedilol (c.f. **Figure 2**), is 50-100 times more potent than carvedilol itself as an antioxidant (due to the fact that a hydroxyl group substitution in a heterocyclic ring increases the ability of that ring to donate electrons)[23,29-31]. Seeing as excessive formation of ROS is associated with ischemia-reperfusion injury found in chronic states of heart failure, carvedilol's ability to prevent and improve IHD is a result of its antioxidant effect[29].

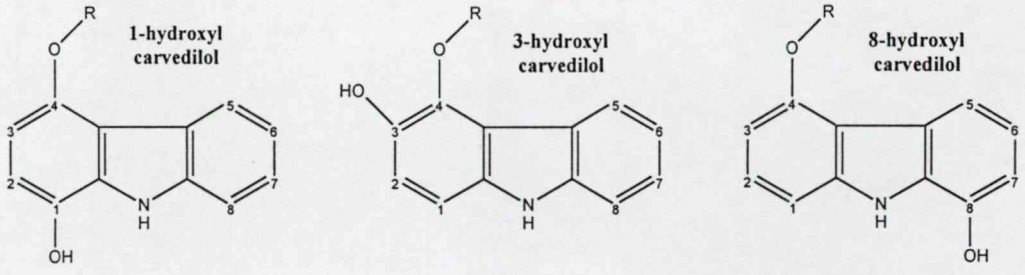

Figure 2: Molecular structure of carvedilol's antioxidant-marked metabolites (biotransformed *via* ring hydroxylation). Note that all metabolites are devoid of either α_1- or β_1/β_2-adrenergic blocking activity. (R depicts rest of carvedilol structure; IUPAC numbering used.)

Carvedilol improves glucose and lipid metabolism in hypertensive patients that display insulin-resistance and hyperinsulinemia (reduction in insulin sensitivity) *via* its effects on peripheral blood flow caused by the combination of β- and α_1-adrenoceptor blockade and antioxidant action[1,32-34]. With regards to electrophysiological effects, carvedilol produces a moderate prolongation of action potential duration (APD) through inhibition of: L-type Ca^{2+} inward currents, delayed rectifier K^+ currents (rapidly and slowly activating components), and transient outward K^+ currents[12]. Extended APD is effective in the treatment of tachyarrhythmias and in patients with post myocardial infarction (MI) or CHF[35].

Due to the above pharmacodynamics, carvedilol acts as a multi-faceted cardioprotector possessing: anti-proliferative (inhibits proliferation by mitogens such as growth factors and angiotensin II)[36], anti-atherogenic (inhibits abnormal smooth muscle growth)[37], anti-ischemic (limits reperfusion injury)[38,39], anti-hypertrophic (reduces left ventricle and vascular hypertrophy involved in cardiac remodeling and myopathies)[40-42], and anti-arrhythmic (prevents ventricular tachyarrhythmias) actions[43-45].

Antioxidant cardioprotection by carvedilol occurs in the mitochondria by mild uncoupling of oxidative phosphorylation *via* the protonable amino group of its side-chain[11]. An uncoupler exerts its effects by eliminating the essential mitochondrial proton gradient by freely exchanging protons across the mitochondrial membranes[46]. It is proposed that the amino group of carvedilol (pK_a = 7.9) binds a proton in the low pH intermembrane space, crosses the membrane in the positively-charged protonated form into the relatively higher pH mitochondrial matrix (driven by its high lipid solubility and the electric potential which is negative in the matrix with regards to the intermembrane space), releases the proton in the matrix, and then returns to the cytosolic leaflet in the deprotonated neutral from[11]. The phenomenon known as "mild uncoupling" occurs when a small decrease in mitochondrial electric potential induces a reduction in the ROS produced by the mitochondrial respiratory chain, thereby producing protective effects[11,47,48].

It has been shown that carvedilol and its active hydroxylated analogues act as novel anti-fibrillar agents able to inhibit Aβ fibril formation[15]. According to the amyloid cascade hypothesis of Alzheimer's disease (AD), accumulation of Aβ in extracellular senile plaques (SPs) in brain tissues drives AD pathogenesis[49]. The culprits of these processes are Aβ peptides consisting of 42 or 43 amino acids

(abbreviated as Aβ1-42) which are prone to aggregation, oligomerization, and deposition in diffuse plaques causing progressive synaptic and neuritic injury[49,50]. Recently, it has been shown that Aβ oligomers (dimers, trimers, or higher oligomers), in the absence of monomers and amyloid fibrils, are the main neurotoxic component of AD[51-54]. Given the above, as an anti-fibrillar agent, carvedilol may have uses in the prevention or slowing down of AD pathology. The effectiveness of carvedilol's inhibition of Aβ fibril formation is due to three factors: (1) a central basic amino pharmacophore, (2) two cyclic hydrophobic ring centroids, and (3) the molecular flexibility to adopt a specific three-dimensional pharmacophore conformation[15]. Although these three factors are elucidated, it is currently not known if carvedilol binds to Aβ monomers, dimers, or other oligomers[15] or what type of interaction occurs between carvedilol and the Aβ peptide(s).

A schematic summary of the biological and pharmacodynamic properties of carvedilol is displayed in **Figure 3**. Given carvedilol's varied pharmacodynamic profiles and the lack of structural information available, this work attempts to divulge carvedilol's complete molecular and conformational identity as a fundamental means to gain a superior comprehension of its biological and physiological mechanisms and endpoints.

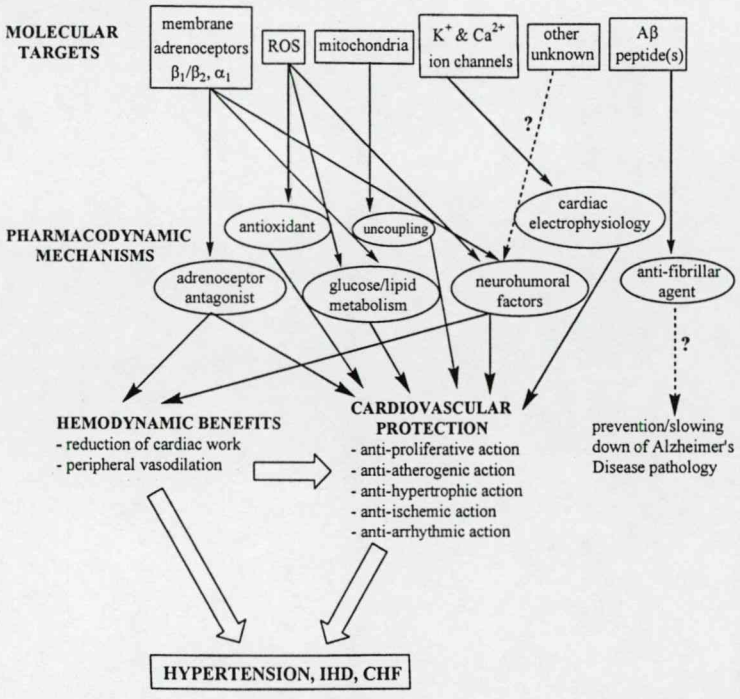

Figure 3: Molecular targets, pharmacodynamic mechanisms, hemodynamic benefits, cardiovascular protection, and physiological endpoints of carvedilol (adapted from reference **1**).

1.2 Stereogenic Units of Carvedilol

Carvedilol exists as a racemic mixture of both enantiomers *R*(+) and *S*(-)[22]. However, carvedilol's enantiomers show marked stereoselective properties in that both stereoisomers have equal α_1-adrenoceptor blocking activity but only the *S*(-) enantiomer possesses the nonselective β-adrenergic antagonist activity[8]. This represents an unusual situation in which enantiomers of an optically active drug differ not only quantitatively in terms of potency but also qualitatively in that they possess distinct pharmacologic profiles[55].

The importance of point chiral stereogenic units (*R* and *S*) is widely accepted in bio-organic chemistry. Point chiral enantiomers have the same physical properties but can produce different biological effects in asymmetrical molecular environments [e.g., β-adrenergic receptor antagonism by *S*(-) carvedilol]. Contrasting, enantiomers may also produce identical biological effects when they interact with a symmetrical molecular environment (e.g., both enantiomers of carvedilol have equal α_1-adrenergic antagonist capabilities and antioxidant activity).

However, not only an asymmetric centre can act as a stereogenic unit but an axis as well. Axis chirality, resulting from a clockwise or counter-clockwise conformational twist, is an important phenomenon in the field of chirality[56-58]. Axis chirality occurs when molecular structures adopt conformations with asymmetrical electron distributions; for a given pro-chiral or point chiral structure, an asymmetric molecular formation (e.g., *gauche* plus, *g*+) will have an energetically equivalent conformation with the corresponding axis chirality (e.g., *gauche* minus, *g*-). Axis chirality may play a significant role in molecular recognition or in docking at chiral active sites of enzymes or receptors.

In assuming a unified viewpoint, one might say that optical isomerism provides evidence about the chiral disposition of electron density in space around the nuclei. The chirality of the electron density exists irrespective of whether it is associated with a carbon carrying four different substituents (point chirality) or if it is associated with the asymmetric electron distribution caused by a conformational twist (axis chirality). Since chirality is central to the structure of any molecular system, the stereogenic units of carvedilol will be investigated to highlight the presence of point and axis chirality and explain how both can be used to predict the electronic structure and energetics of corresponding chiral minima.

2. CHOICE OF TOPIC

Carvedilol possesses wide-ranging pharmacodynamics with therapeutic potential in cardiovascular physiology, oxidative stress, and neurodegenerative processes. However, essential comprehension of carvedilol's gas and solvent phase conformational preferences – with emphasis on the electronic structure of its low energy states because, according to basic thermodynamics, only low energy states will be significantly occupied[59] – is relatively unknown. The X-ray diffraction crystal structure of carvedilol, developed by Chen and coworkers[60], displays only neutral enantiomer structure and does not elucidate any structural parameters of single-molecule protonated carvedilol. This lacks full relevance to carvedilol as its mechanisms of action ultimately involve one molecule interacting with a respective molecular target.

As such, it is evident that revealing carvedilol's full structural profile including: stereochemical relationships, basicity, and highly populated conformations, is indispensable to expounding the molecular basis of its adrenoceptor binding conformation, cardiovascular mechanisms, role in antioxidant pathways, uncoupling of oxidative phosphorylation in mitochondria, and interaction with Aβ peptide(s) since structure and conformation is a requisite and fundamental part of all of these processes. This work will exhaustively consider and examine carvedilol's electronic structure using theoretical quantum chemical and experimental nuclear magnetic resonance (NMR) spectroscopy methods to resolve the preferred conformations of carvedilol's potential energy hypersurface (PEHS).

Given carvedilol's 11 torsional angles and 177 147 (3^{11}) conformational possibilities (total is arrived at by means of multi dimensional conformation analysis [MDCA] where each torsional angle can assume *gauche plus*, *anti*, or *gauche minus* orientations), it is clear that this is a extensive and laborious task by conventional MDCA or random PEHS sampling. Consequently, carvedilol provides an exceptional opportunity to develop an original theoretical methodology to investigate such multifarious and dynamic molecular systems in great detail with minimal resource cost. Thus, the choice of analyzing carvedilol is twofold: reveal its dominant conformations to improve molecular understanding of its pharmacodynamics and develop a novel theoretical method to discern the low energy states of molecular systems with exorbitant conformational possibilities.

3. AIM OF STUDY

This dissertation is carried out with a fourfold aim: (1) devise a novel structure-activity fragmentation method with substantial predictive power and minimal computational cost to assess and analyze the conformations of selected carvedilol molecular fragments and to predict the conformations of carvedilol; (2) evaluate the stereochemical relationships, emphasizing point chirality and axis chirality, of carvedilol since its pharmacologic profiles are unique in their stereochemical reliance; (3) examine the dependence of basicity (proton affinity) on conformation as is relevant to carvedilol's role as a physiological base in mitochondria uncoupling; (4) discover, determine, and depict the electronic structure of carvedilol's most populated (lowest energy) conformations expected to dominate physical and biological samples.

Gas and solvent phase theoretical *ab initio* and density functional theory (DFT) quantum chemical molecular orbital (MO) computations will be employed for the development of the rational molecular fragmentation method and for all carvedilol and fragment structural, stereochemical, and proton affinity investigations. Additionally, MO computations will be used to gauge the accuracy and ability of the devised method to predict the preferred conformations of carvedilol. NMR spectroscopy will be utilized for the structural analysis of carvedilol, to compare experimentally- and theoretically-determined structures, and to further assess the success of the molecular fragmentation approach.

The comprehensive solution of carvedilol's conformational character and related structural parameters will greatly aid the molecular discernment of its role in adrenoceptor binding, effects on adrenergic neurotransmission, and in ameliorating pathological states such as oxidative stress and AD. Furthermore, satisfactory success of the application of this developed rational molecular fragmentation method for the structural analysis of carvedilol may indicate its viability for the study of other complex molecular systems with regards to broad prediction and analysis of electronic structure, stereochemical, and conformational parameters.

4. METHODS

4.1 Rational Molecular Fragmentation of Carvedilol

The molecular fragmentation of carvedilol is based on the rational deconstruction of carvedilol's chemical structure into structure-activity regions as a means to create molecular fragments with simplified PEHSs for MDCA conformational analysis; however, the fragments must still retain key elements of the whole structure. Such a creation of fragments directly relevant to the whole molecule is necessary for the precise extrapolation of electronic structure and intramolecular attractive forces (IMAF) from the individual fragments to carvedilol.

From a structural and pharmacological standpoint, the most coherent procedure for fragmentation is pharmacophore-based because the pharmacophore unit represents the critical part (i.e., critical functional groups) of the molecule necessary to confer the observable physiological effect(s). For carvedilol, the latter includes both pharmacophores with affinity (but no intrinsic activity) for a receptor site (e.g., β_1/β_2- and α1-adrenoceptor antagonist) and pharmacophores which do not interact with a specific receptor site but nonetheless produce specific effects (e.g., antioxidant, uncoupling, and Aβ-binding actions). Furthermore, since each fragment will be exhaustively studied by MDCA, it is ideal to have fragments with no more than four torsional angles ($3^4 = 81$ conformational possibilities) as opposed to five dihedrals of interest ($3^5 = 243$ conformational possibilities) to minimize computational resources.

Carvedilol is composed of three distinct pharmacophores: the antioxidant aryloxypropanolamine β_1/β_2-adrenoceptor antagonist, the secondary amine which contains the protonophoretic amino group involved in the uncoupling of mitochondrial oxidative phosphorylation, and the di-substituted benzene α_1-blocker pharmacophore (c.f. **Figure 1**). Hence, carvedilol was divided into three molecular fragments in an attempt to maximize structural resemblance and minimize conformational complexity: *R*- and *S*-4-(2-hydroxypropoxy)carbazol (Fragment A) possesses the carbazole ring and chiral oxypropanol structure, 2(*R* and *S*)-1-(ethylamonium)propane-2-ol (Fragment B) contains the chiral carbon centre and the amino group involved in mitochondria uncoupling and part of the β-blocker portion of carvedilol, and aminoethoxy-2-methoxy-benzene (Fragment C) is the α_1-adrenergic antagonist pharmacophore of carvedilol with a terminal primary amine

(c.f. **Figure 4**). The secondary amine of carvedilol was not included in Fragment A to minimize number of torsional angles and because Fragment B preserves the hydroxyl group/amine orientation found in the carvedilol side-chain.

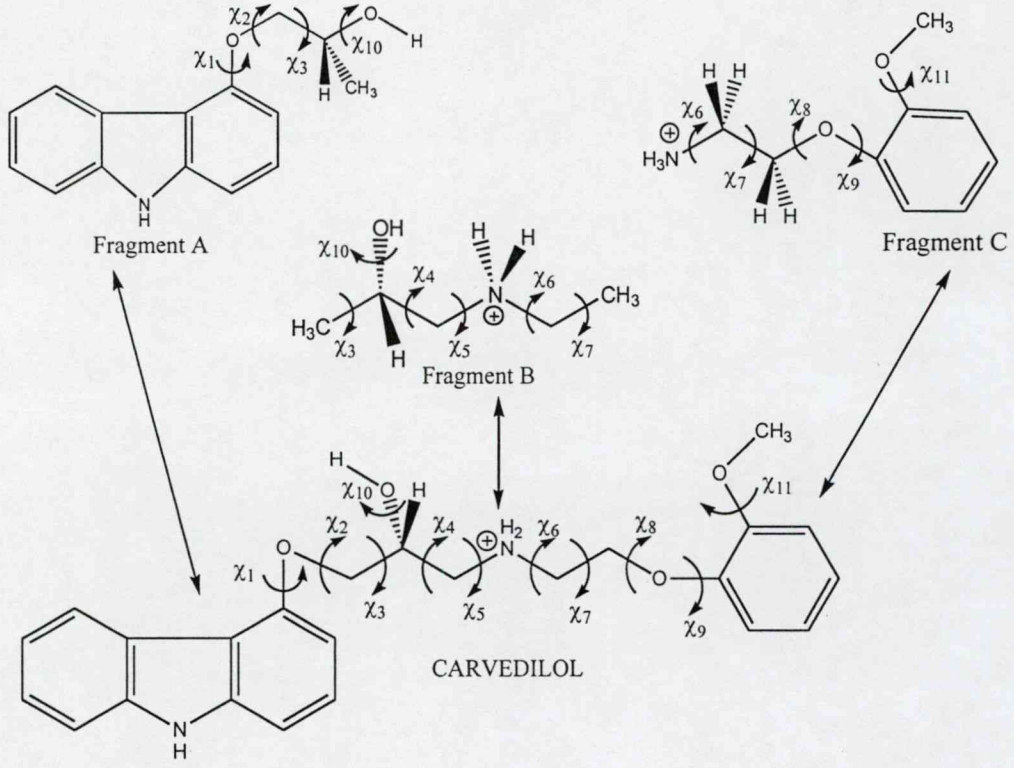

Figure 4: Carvedilol was divided into three molecular fragments based on pharmacophore structure-activity: *R*- and *S*-4-(2-hydroxypropoxy) carbazol (Fragment A), 2(*R* and *S*)-1-(ethylamonium)propane-2-ol (Fragment B), and aminoethoxy-2-methoxy-benzene (Fragment C).

As designed, although the carvedilol fragments contain more than four torsional angles each, only four dihedrals are of interest and to be analyzed by MDCA because each fragment contains extraneous torsional angles with symmetrical rotations that need not be evaluated. The 11 torsional angles of carvedilol are represented in the three fragments as follows: Fragment A, χ_1, χ_2, χ_3, χ_{10}; Fragment B, χ_4, χ_5, χ_6, χ_{10}; and Fragment C, χ_7, χ_8, χ_9, χ_{11}.

The central ideology of the rational molecular fragmentation method applied to carvedilol is as follows: if carvedilol, a molecule with many degrees of freedom (i.e., a large conformational hypersurface), is divided into simpler structural fragments (e.g., Fragments A, B, and C) with manageable PEHSs, but still relevant to the electronic structure of the whole molecule, then these smaller structures can

be thoroughly analyzed by MDCA whereas carvedilol cannot. The fragments, once optimized and evaluated (i.e., dominant conformations revealed), can be used to hypothesize the low energy conformations of carvedilol itself. Since only the low energy states pertaining to each fragment are used, they should ultimately lead to the discovery of corresponding low energy carvedilol conformations. The hypothesized low energy carvedilol conformations are then tested and verified with high level gas and solvent phase theoretical optimizations as well as NMR spectroscopy. The theoretical and experimental methods will serve to both expose carvedilol's most populated states and assess the fragmentation method.

4.2 Carvedilol Torsional Angle Definitions

To allow explicit definition and prediction of conformation, a systematic numbering system is used for all structures such that corresponding torsional angles in fragments and carvedilol are all defined in the same orientation. With respect to the carvedilol fragments, Fragment A, B, and C constitute their respective PEHSs as described by equations **[1]**, **[2]**, and **[3]**, respectively (c.f. **Figure 5**). With four torsional angles and three possible minima for each torsional angle (*g*+, *a*, and *g*-), each fragment can theoretically adopt a grand total of 81 (3^4) possible conformational minima. All PEHS conformers of carvedilol are described by equation **[4]** (c.f. **Figure 6**). Finally, conformational assignments for converged minima are made according to equation **[5]** based on the general observation that, if one were to rotate a tetrahedral carbon against another tetrahedral carbon, the minima would generally fall within the above ranges. (All stereochemistry is described below in section **4.3.3 Stereochemical Calculations**.)

$$E = (\chi_1, \chi_2, \chi_3, \chi_{10}) \quad [1]$$

$$E = (\chi_4, \chi_5, \chi_6, \chi_{10}) \quad [2]$$

$$E = (\chi_7, \chi_8, \chi_9, \chi_{11}) \quad [3]$$

$$E = f(\chi_1, \chi_2, \chi_3, \chi_4, \chi_5, \chi_6, \chi_7, \chi_8, \chi_9, \chi_{10}, \chi_{11}) \quad [4]$$

gauche plus (*g*+)	= 60. (ideal) ± 60°	**[5]**
anti (*a*)	= 180. (ideal) ± 60°	
gauche minus (*g*-)	= -60. (ideal) ± 60°	

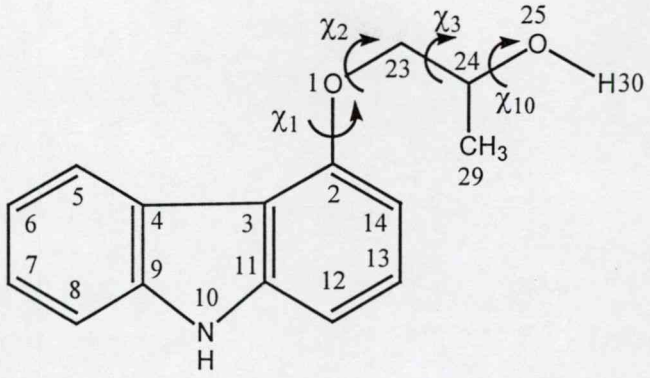

χ_1 = C23-O1-C2-C3 χ_3 = C29-C24-C23-O1

χ2 = C24-C23-O1-C2 χ_{10} = H30-O25-C24-C23

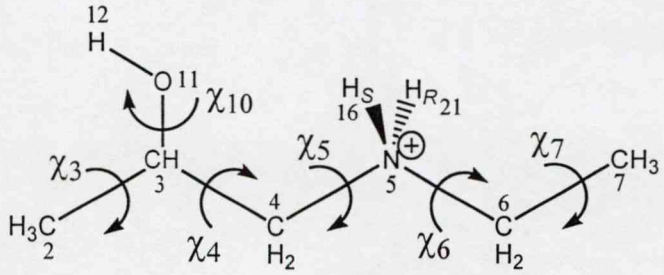

χ_4 = N5-C4-C3-C2 χ_6 = C7-C6-N5-C4

χ_5 = C6-N5-C4-C3 χ_{10} = H12-O11-C3-C2

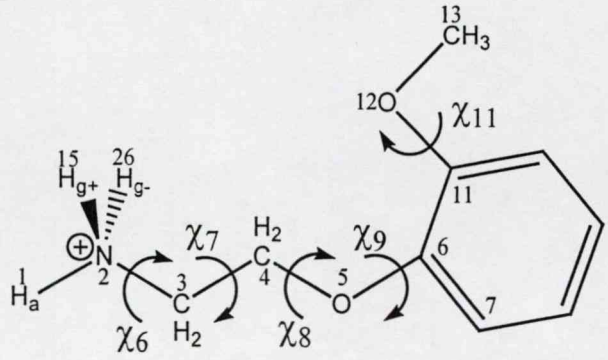

χ_7 = O5-C4-C3-N2 χ_9 = C7-C6-O5-C4

χ_8 = C6-O5-C4-C3 χ_{11} = C13-O12-C11-C6

Figure 5: Numbering and definition for torsional angles of interest pertaining to Fragment A (stereocentre located at centre C24), Fragment B (stereocentre located at centre C3), and Fragment C. Numbers placed beside atoms indicates numbering used as input for GAUSSIAN98.

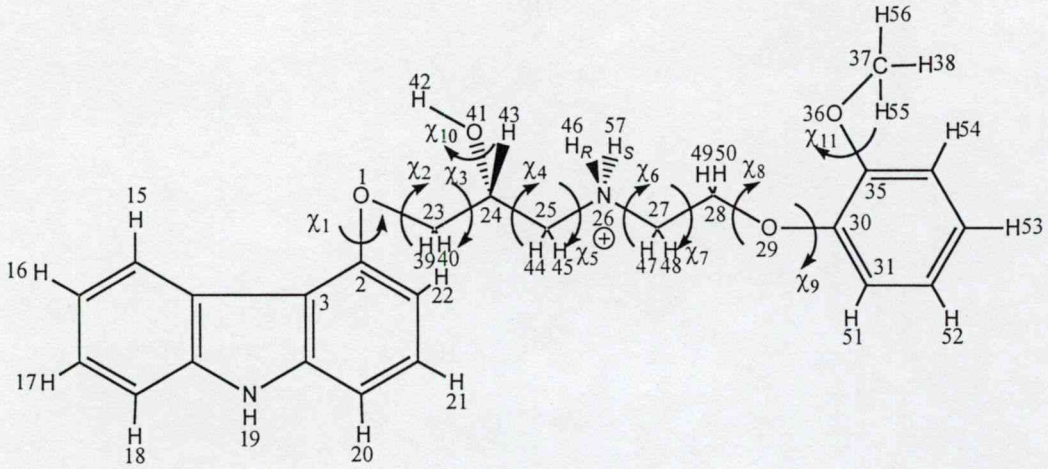

χ_1 = C23, O1, C2, C3 χ_2 = C24, C23, O1, C2 χ_3 = C25, C24, C23, O1

χ_4 = N26, C25, C24, C23 χ_5 = C27, N26, C25, C24 χ_6 = C28, C27, N26, C25

χ_7 = O29, C28, C27, N26 χ_8 = C30, O29, C28, C27 χ_9 = C31, C30, O29, C28

χ_{10} = H42, O41, C24, C23 χ_{11} = C37, O36, C35, C30

Figure 6: Molecular structure of N-protonated *R*-carvedilol and all torsional angle definitions used. Numbers placed beside atoms were used to define *R*-carvedilol for GAUSSIAN98 and for NMR spectroscopic analysis.

4.3 Gaussian Computations

4.3.1 Gas Phase Calculations

All quantum chemical molecular orbital (MO) calculations were carried out using the GAUSSIAN98 (G98) software program[61]. Carvedilol molecular fragments and *R*-carvedilol were exclusively defined using the G98 Cartesian and z-matrix internal coordinate system to specify molecular structure, stereochemistry, and geometry[61].

Fragment A was initially studied with MO calculations of its PEHS conformational minima. Full MDCA geometry optimizations were performed in the gas phase (ε = 0.0) successively at the restricted Hartree-Fock, RHF/3-21G and RHF/6-31G(d), levels of theory and then using DFT with the Becke 3LYP hybrid exchange-correlation functional[62] at the B3LYP/6-31G(d) level of theory. Vibrational frequency calculations were performed on all minima at the B3LYP/6-31G(d) level of theory to ensure that the optimized conformers were true minima and contained no imaginary frequencies. Three levels of theory were utilized for the

analysis of the Fragment A PEHS to ensure only legitimate conformations were revealed because it is expected that the bulky carbazole aromatic ring will be difficult to optimize and that it will seriously influence the conformational preferences of both Fragment A and whole carvedilol. As such, a reliable foundation of the electronic structural parameters and IMAF of the carbazole ring and this carvedilol fragment is desired.

Structural analysis of Fragment B and C were computed by MDCA of their respective PEHSs with optimizations of the conformational minima at the RHF/3-21G level of theory. Only HF was employed for the analysis of Fragment B and C because of their inherently simpler chemical structures compared to Fragment A. Separate energies of deprotonation were calculated for the secondary amine of Fragment B and the primary amine of Fragment C to account for the role of conformation-dependent basicity as related to carvedilol's role in the uncoupling of mitochondria oxidative phosphorylation (c.f. **4.3.4 Proton Affinity & Conformational Basicity Calculations** below).

To arrive at only significantly populated, low energy conformations of carvedilol, only converged Fragment A, B, and C structures with a conformer relative energy $\leq$ 2.00 Kcal•mol^{-1} were selected for carvedilol conformer predictions. This selection criterion utilizes low energy fragment geometries to predict, *via* non-redundant conformational permutations, hypothesized low energy conformations of *R*-carvedilol. All *R*-carvedilol conformational predictions were tested with full geometry optimizations in the gas phase at the RHF/3-21G level of theory using the predicted conformations as input geometries.

Subsequently, the conformations and relative energies of the *R*-carvedilol converged structures were analyzed to select a non-arbitrary, definite set of low energy structures. This set of structures was further optimized in the gas phase at the B3LYP/6-31G(d) level of theory; i.e., inputs for these DFT calculations were the RHF/3-21G optimized coordinates. High level DFT calculations were carried out on these focal low energy carvedilol conformations to ensure the finest possible description of electronic structure was achieved. All graphical data was plotted using Axum 5.0[63] and Excel[64].

4.3.2 Solvent Phase Calculations

In biological samples, the dominant states of carvedilol will occur in solvent environments, it is thus essential to characterize the electronic structure and energetics of solvent optimized conformers. Consequently, DFT gas phase optimized geometries, belonging to the set of low energy conformers, were used as input for DFT self-consistent reaction field (SCRF) calculations to illustrate the solvent effect (solvent-induced change in energy difference) of carvedilol.

To begin with, independent molecular volume calculations were computed on all gas phase DFT converged structures to estimate a solute radius (a_0) for use with the theoretical solvent method. Once the solute radii had been calculated, the Onsager solvent reaction field method[65-70] was utilized at the B3LYP/6-31G(d) level of theory to optimize all structures in aprotic dimethyl sulfoxide (DMSO; $\varepsilon = 46.70$) and protic water ($\varepsilon = 78.39$) solvents. The Onsager method places the solute in a fixed spherical cavity, defined by the solute radius, within the solvent field[71]. Net stabilization is achieved corresponding to the interactions between the molecular dipole (which induces a dipole in the solvent medium) and the electric field applied by the solvent dipole[71]. To satisfy the need of quantitatively-significant results, the self-consistent field (SCF) "tight" option was utilized for volume and Onsager calculations for a more accurate integration by means of an increase in the density of points used.

4.3.3 Stereochemical Calculations

To a certain extent, as described above (c.f. **1.2 Stereogenic Units of Carvedilol**), carvedilol's pharmacology is stereochemically-dependent. To explore how chiral electron density and optical isomerism can be exploited to predict properties of stereoisomers, the axis and point chirality of carvedilol was investigated with MO calculations of Fragment A and selected chiral and achiral analogues. Fragment A was chosen because it is considered to be the most difficult carvedilol fragment to optimize; as a result, if it is possible to satisfactorily predict the stereochemical relationships of this fragment, the methodology and results can be extrapolated and applied to carvedilol Fragment B (possesses point and axis chirality), Fragment C (possesses axis chirality) and whole carvedilol (possesses point and axis chirality).

Stereochemical calculations focus on the gas phase MDCA of both *R*-4-(2-hydroxypropoxy)carbazol (*R*-Fragment A) and *S*-4-(2-hydroxypropoxy)carbazol (*S*-Fragment A) along with six analogue structures: (2-hydroxyethoxy)carbazol (II-H_2), (2-hydroxy-2-methyl-ethoxy)carbazol (II-Me_2), (2*R*)-1-methoxypropan-2-ol (III-[H,Me]-*R*), (2*S*)-1-methoxypropan-2-ol (III-[H,Me]-*S*), 2-methoxyethan-1-ol (IV-H_2), and 1-methoxy-2-methyl-propane-2-ol (IV-Me_2) (c.f. **Figure 7**). Full geometry optimizations were performed on all structures in **Figure 7** at the RHF/3-21G, RHF/6-31G(d), and B3LYP/6-31G(d) levels of theory.

Structures IV-H_2, IV-Me_2, III-[H,Me]-*S*, and III-[H,Me]-*R* were constructed by replacing the bulky carbazole ring system with the simplest alkyl group, a methyl substituent. The backbone present in carvedilol, and in *R*- and *S*-Fragment A, remained in all structures with the exceptions that IV-H_2 was devoid of the methyl group formerly present at the chiral centre while IV-Me_2 was constructed with two methyl groups at the former chiral centre, and consequently, both of these analogues are achiral. Structures III-[H,Me]-*R* and III-[H,Me]-*S* retained the chirality present in carvedilol. Analogues II-H_2 and II-Me_2 were constructed in the same manner as IV-H_2 and IV-Me_2 with the exception that the carbazole ring was maintained. As such, II-H_2 and II-Me_2 are achiral representative structures of *R*- and *S*-Fragment A.

As a group, the structures presented in **Figure 7** should allow assessment of the stereochemical properties pertaining to all fragments and carvedilol because they represent different variants of the carvedilol stereocentre with point chiral (*R*- and *S*-Fragment A, III-[H,Me]-*S*, and III-[H,Me]-*R*) and pro-chiral (IV-H_2, IV-Me_2, II-H_2, and II-Me_2) designations. Pro-chiral structures will disclose the basis of axis chirality while point chiral structures will divulge both the axis and point chiral relationships of carvedilol. MDCA at various levels of theory is preferred to outline the stereochemistry of carvedilol and its fragments because an exhaustive approach that evaluates all valid conformations of a respective PEHS is necessary.

Finally, to ensure that all fragments correspond stereochemically with each other and carvedilol (i.e., torsional angle χ_{10} has the same orientation in all structures), only the B3LYP/6-31G(d) results of *R*-Fragment A, RHF/3-21G results of *S*-Fragment B, and RHF/3-21G results of Fragment C will be used for the conformational predictions of *R*-carvedilol.

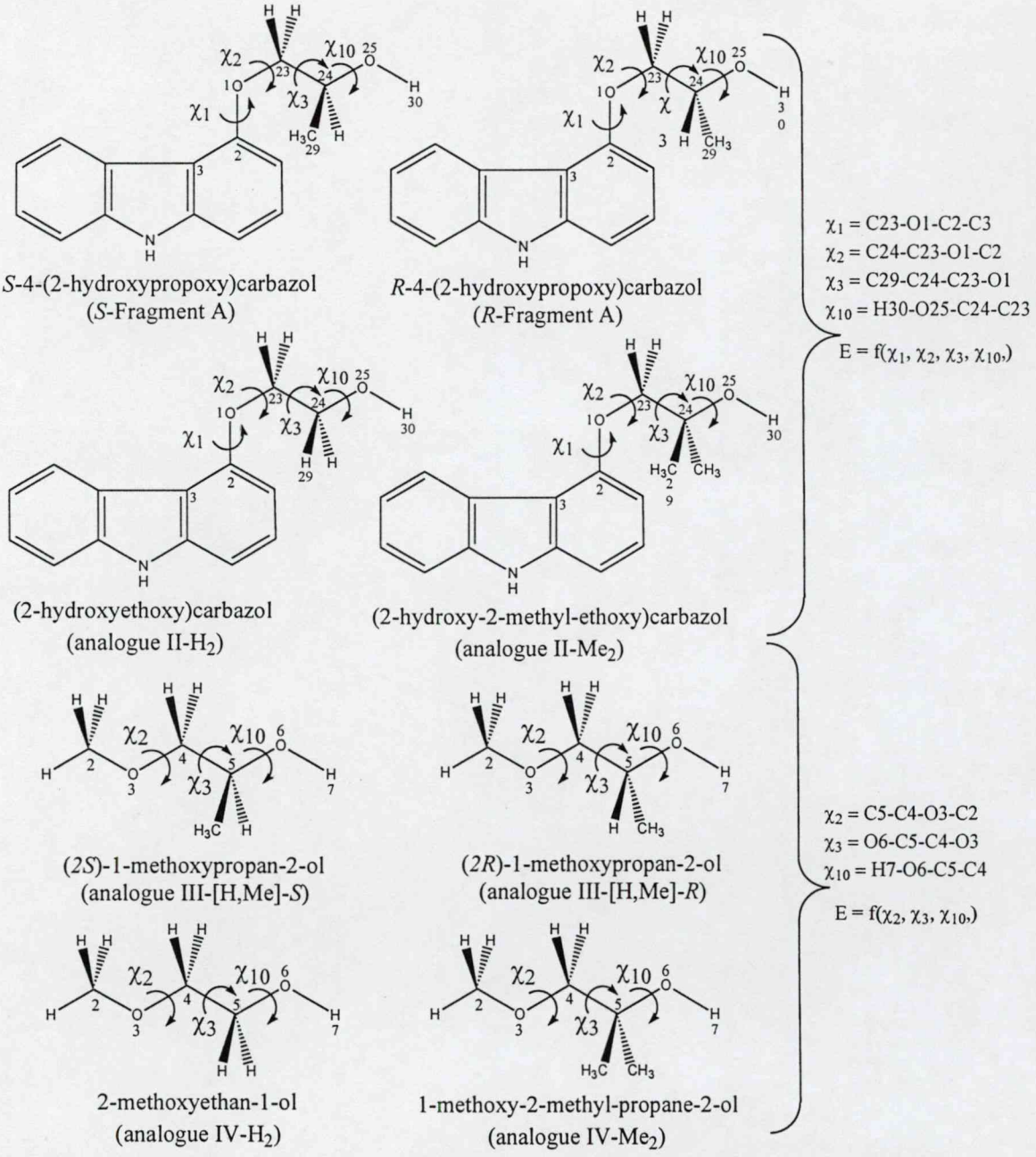

Figure 7: Numbering and definition of torsional angles for *S*- and *R*-Fragment A along with analogues II-H_2, II-Me_2, III-[H,Me]-*S*, III-[H,Me]-*R*, IV-H_2, and IV-Me_2. All structures were optimized at the RHF/3-21G, RHF/6-31G(d), and B3LYP/6-31G(d) levels of theory to illustrate the stereochemical relationships of carvedilol and its fragments. Numbers placed beside atoms indicates numbering used for GAUSSIAN98.

4.3.4 Proton Affinity & Conformational Basicity Calculations

Previous work by Koo *et al.*[72] has shown that the intrinsic acidity of the aspartic acid residue side-chain is dependent on conformation. Likewise, carvedilol, as a physiological base (pK_a = 7.9), is expected to have its basicity influenced by conformation as related to its uncoupling mechanism in mitochondria. However, whereas a monoprotic acid can only be deprotonated by way of one proton, the secondary amines carvedilol and Fragment B depict the phenomena where a molecule can be deprotonated *via* the abstraction of either one of two protons. The latter is evident when either of the two protons is replaced by deuterium which leads to a nitrogen centre with either an *S*- or *R*-configuration, depending on which proton is replaced with deuterium; the protons are denoted as H_S (H16) and H_R (H21) in **Figure 5**. This designation may also be applied to deprotonation schemes; for example, deprotonation of H_S would leave the nitrogen centre with H_R bonded and possessing an *R*-configuration. Therefore, it is hypothesized that, dependent on the conformations adopted by Fragment B (and carvedilol accordingly), H_S and H_R will require different energies of deprotonation. Previous proton affinity studies for carvedilol reveal energies of deprotonation between 234 and 238 kcal•mol^{-1} but do not discriminate the different protons[11].

To increase the complexity of this deprotonation phenomenon, the primary amine Fragment C can be deprotonated *via* the removal of one of three protons. If any of these protons were replaced with deuterium, one would have deuterium in either of three positions: *anti* position (H1, denoted as H_a), the *g*+ position (H15, denoted as H_{g+}), or the *g*- position (H26, denoted as H_{g-}) (c.f. **Figure 5**). Analysis of the conformational-dependent basicity of Fragment B and C is relevant for two reasons: (1) revealing the extent conformation influences basicity has implications in carvedilol's uncoupling mechanism; (2) comparing the dependence of basicity on conformation for a primary (Fragment C) and secondary (Fragment B) amine is a complete analysis of multiple proton conformational basicity because such a challenge does not occur for tertiary amines as only one proton can be abstracted (analogous to monoprotic acids) and neither for quaternary ammonium compounds because of the lack of protons at the nitrogen centre.

For Fragment B, a separate two prong conformational methodology was applied to analyze the intrinsic basicity of the amino group (c.f. **Figure 8**). For each

converged conformation, protonated Fragment B (BH^+) was independently deprotonated of protons H_S and H_R. Initially, vertical proton affinities were calculated, denoted as $\Delta E_{vert}(S)$ and $\Delta E_{vert}(R)$ for H_S and H_R deprotonations, respectively, with single-point energy (SPE) calculations (c.f. equation **[6]** and **[7]**). The deprotonated Fragment B (B) structures were then optimized and adiabatic proton affinities (process in which the geometries are relaxed) were calculated. These values, denoted as $\Delta E_{opt}(S)$ and $\Delta E_{opt}(R)$, represent H_S and H_R optimized energies of deprotonation, respectively (c.f. equation **[8]** and **[9]**). A third value, denoted as $\Delta\Delta E(S)$ and $\Delta\Delta E(R)$, represents the difference between the SPE [$\Delta E_{vert}(S)$ and $\Delta E_{vert}(R)$] and the optimized [$\Delta E_{opt}(S)$ and $\Delta E_{opt}(R)$] values for the energies of deprotonation for each conformer (c.f. equation **[10]** and **[11]**). This latter set of values can be interpreted as the stabilization experienced by Fragment B conformers as they adopted an optimized conformation after deprotonation.

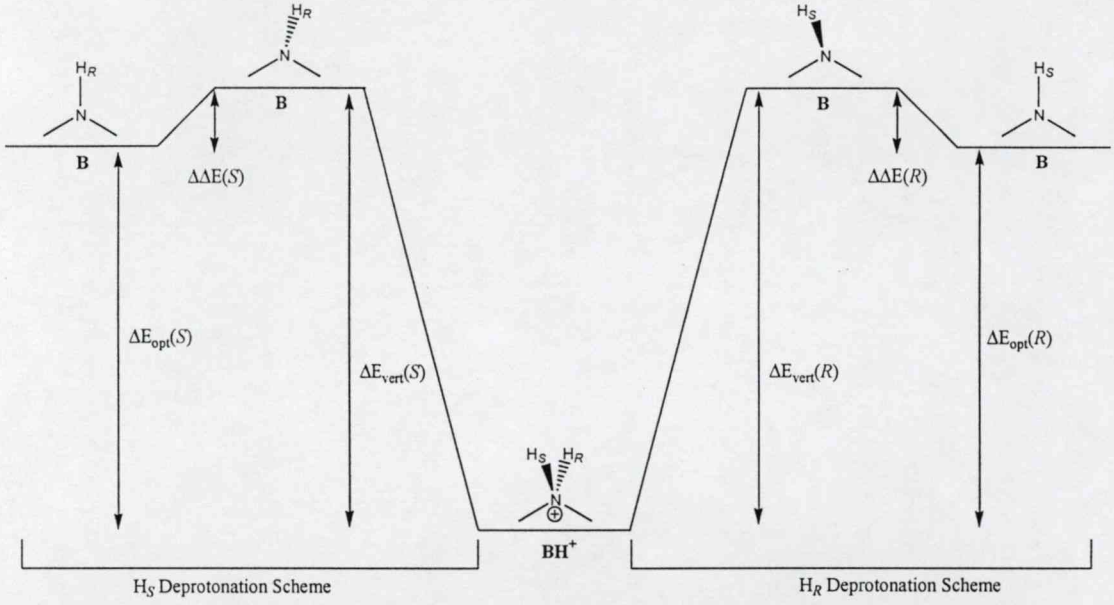

Figure 8: Two prong methodology employed to analyze the conformational-dependent basicity of the amino group of Fragment B.

$$\Delta E_{vert}(S) = |E_{opt}[BH^+] - E_{SP}[B]| \quad (H_S \text{ deprotonation}) \quad \textbf{[6]}$$

$$\Delta E_{vert}(R) = |E_{opt}[BH^+] - E_{SP}[B]| \quad (H_R \text{ deprotonation}) \quad \textbf{[7]}$$

$$\Delta E_{opt}(S) = |E_{opt}[BH^+] - E_{opt}[B]| \quad (H_S \text{ deprotonation}) \quad \textbf{[8]}$$

$$\Delta E_{opt}(R) = |E_{opt}[BH^+] - E_{opt}[B]| \quad (H_R \text{ deprotonation}) \quad \textbf{[9]}$$

$$\Delta\Delta E(S) = \Delta E_{vert}(S) - \Delta E_{opt}(S) \quad (H_S \text{ deprotonation}) \quad \textbf{[10]}$$

$$\Delta\Delta E(R) = \Delta E_{vert}(R) - \Delta E_{opt}(R) \qquad (H_R \text{ deprotonation}) \qquad \textbf{[11]}$$

Converged structures of protonated Fragment C (CH^+) were independently deprotonated of protons H_a, H_{g+}, and H_{g-} and the vertical energies of deprotonation were calculated with SPE calculations. These energy values are denoted as $\Delta E_{vert}(a)$, $\Delta E_{vert}(g+)$, and $\Delta E_{vert}(g-)$ (c.f. equation **[12]**, **[13]**, and **[14]**). The H_a, H_{g+}, and H_{g-} deprotonated Fragment C (C) conformers were then optimized and adiabatic energies of deprotonation calculated; denoted as $\Delta E_{opt}(a)$, $\Delta E_{opt}(g+)$, and $\Delta E_{opt}(g-)$ (c.f. equation **[15]**, **[16]**, and **[17]**). The values denoted as $\Delta\Delta E(a)$, $\Delta\Delta E(g+)$, and $\Delta\Delta E(g-)$ represent the differences between vertical and optimized adiabatic energies of deprotonation for each conformer (c.f. equation **[18]**, **[19]**, and **[20]**). This methodology is illustrated in **Figure 9**. A positive value for the energy of deprotonation appears because bond-breaking is always an endothermic process.

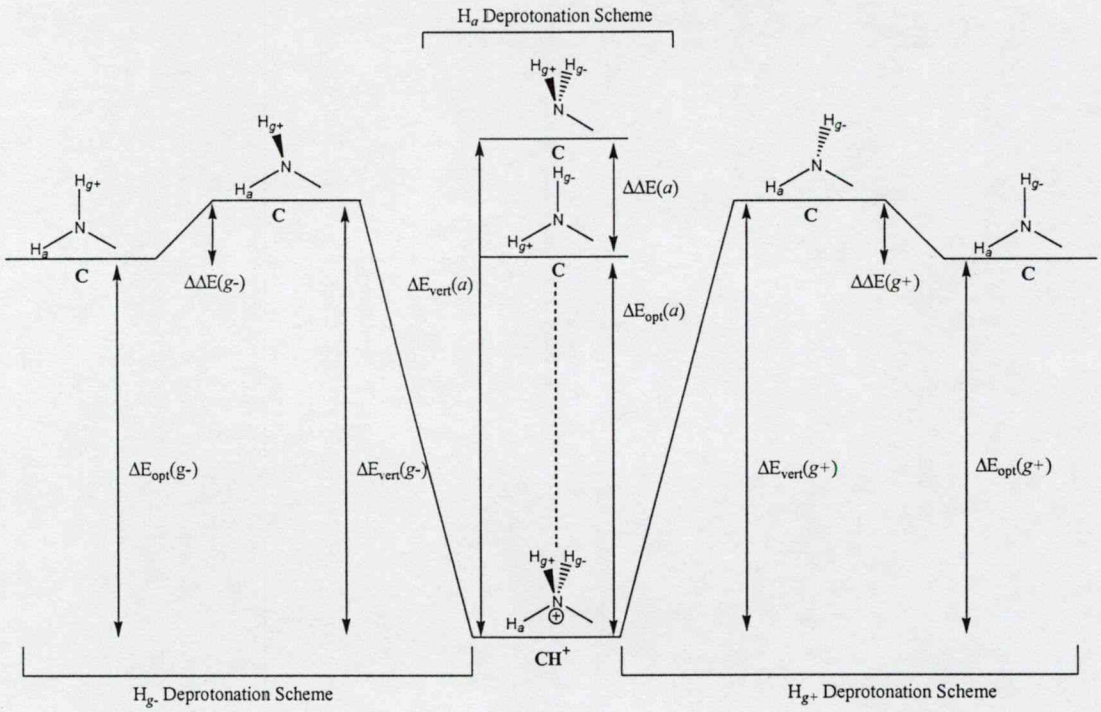

Figure 9: Three prong methodology utilized to analyze the dependence of basicity on conformation of the amino group of Fragment C.

$$\Delta E_{vert}(a) = |E_{opt}[CH^+] - E_{SP}[C]| \qquad (H_a \text{ deprotonation}) \qquad \textbf{[12]}$$

$$\Delta E_{vert}(g+) = |E_{opt}[CH^+] - E_{SP}[C]| \qquad (H_{g+} \text{ deprotonation}) \qquad \textbf{[13]}$$

$$\Delta E_{vert}(g-) = |E_{opt}[CH^+] - E_{SP}[C]| \qquad (H_{g-} \text{ deprotonation}) \qquad \textbf{[14]}$$

$$\Delta E_{opt}(a) = |E_{opt}[CH^+] - E_{opt}[C]| \quad (H_a \text{ deprotonation}) \quad [15]$$

$$\Delta E_{opt}(g+) = |E_{opt}[CH^+] - E_{opt}[C]| \quad (H_{g+} \text{ deprotonation}) \quad [16]$$

$$\Delta E_{opt}(g-) = |E_{opt}[CH^+] - E_{opt}[C]| \quad (H_{g-} \text{ deprotonation}) \quad [17]$$

$$\Delta\Delta E(a) = \Delta E_{vert}(a) - \Delta E_{opt}(a) \quad (H_a \text{ deprotonation}) \quad [18]$$

$$\Delta\Delta E(g+) = \Delta E_{vert}(g+) - \Delta E_{opt}(g+) \quad (H_{g+} \text{ deprotonation}) \quad [19]$$

$$\Delta\Delta E(g-) = \Delta E_{vert}(g-) - \Delta E_{opt}(g-) \quad (H_{g-} \text{ deprotonation}) \quad [20]$$

4.4 Experimental NMR Spectroscopy Methods

A total of 47.7 mg of carvedilol (purchased from ChemPacific Corporation, Baltimore, Maryland, United States) was dissolved in 550 µl of deuterated DMSO (DMSO-d_6) solvent. All of the spectra were obtained on a Bruker DRX 400 MHz NMR spectrometer at 298 Kelvin using tetramethylsilane (TMS) as a reference at zero parts per million (ppm). Proton chemical shifts were analyzed with decoupled, COSY (correlated spectroscopy), NOESY (nuclear Overhauser enhancement spectroscopy), and ROESY (rotational Overhauser enhancement spectroscopy) spectra. Mixing time was modulated in NOESY experiments for best signal-to-noise ratio in NOE build up curves. All 2D spectra were zero filled once in both dimensions.

Reasons for choosing DMSO (DMSO-d_6) as the solvent for all NMR spectra are threefold: (1) DMSO is polar solvent which generally destroys weak intramolecular H-bonds, therefore, it is an ideal solvent to test the rigidity of the structure and thereby the strength of any assumed H-bond networks; (2) DMSO is an aprotic solvent preventing the ^1H-^2D exchange with polar protons of the solute (contrary to $CDCl_3$ or D_2O) which allows to obtain information on the chemical shifts of the OH and NH protons; (3) carvedilol NMR spectroscopy in DMSO can be promptly compared with DFT optimizations in DMSO available with the G98 software program.

5. RESULTS AND DISCUSSION

5.1 MDCA of Individual Carvedilol Fragments

5.1.1 Hartree-Fock & Density Functional MDCA of Fragment A

All possible minima for the *S*- and *R*-Fragment A PEHS (structure defined in **Figure 5**) were subjected to gas phase optimizations in a subsequent manner at the RHF/3-21G, RHF/6-31G(d), and B3LYP/6-31G(d) level of theory. All minima were sorted by conformation according to equation **[5]**.

Number of converged minima for *S*- and *R*-Fragment A are, respectively: 36 minima (global minima *g-ag+g+* and *g+ag-g-*) at RHF/3-21G (data not shown), 27 minima (*aaag-* and *aaag+*) at RHF/6-31G(d) (data not shown), and 19 minima (*aaag-* and *aaag+*) at B3LYP/6-31G(d) (c.f. **Table 1** and **2**). The fact that only 19 out of a possible 81 conformational minima (23%) successfully converged at the DFT level of theory indicates the conformational character of Fragment A is relatively rigid and strained. As anticipated, the bulky carbazole centroid limits the number of viable conformations that Fragment A can assume and it is probable that this will be a prevailing trend for whole carvedilol as well.

Structural analysis of *R*-Fragment A reveals intramolecular H-bonding between O1 and H30 as the dominant IMAF. All four of the lowest energy conformers with a relative energy less than two Kcal•mol^{-1}, structures *aaag+*, *aag-g-*, *ag-ag+*, and *g-aag+*, contain an O1-H30 H-bond with distances between 2.2 and 2.4 Angstroms (Å) (c.f. **Figure 10**). Similar H-bonding is also present in conformers: *g-g-g-g-* (5.82 kcal•mol^{-1}, 2.74 Å H-bond), *g-g-ag+* (3.60 Kcal•mol^{-1}, 2.20 Å H-bond), *g+ag-g-* (2.26 Kcal•mol^{-1}, 2.25 Å H-bond), and *g+g+ag+* (5.11 Kcal•mol^{-1}, 2.76 Å H-bond). The O1-H30 H-bond allows the formation of an intramolecular five-membered ring which, in conjunction, confers both electrostatic (*via* the H-bond) and steric (*via* the five-membered ring) relaxation to the side-chain of Fragment A. Stereochemical relationships between the *S*- and *R*-Fragment A configurations is presented below in **5.2.1 Chiral Parameters of Carvedilol Fragment A and Selected Analogues.**

Table 1:
B3LYP/6-31G(d) optimized parameters for the minima of *S*-Fragment A.

Conformational Assignment				χ_1 (degrees)	χ_2 (degrees)	χ_3 (degrees)	χ_{10} (degrees)	Energy (hartree)	Rel E (kcal• mol^{-1})
χ_1	χ_2	χ_3	χ_{10}						
g^+	g^+	g^+	g^+	71.61	86.66	54.09	60.83	-785.829262611	5.82
g^+	g+	a	a	85.32	66.14	179.21	-178.06	-785.827598267	6.86
g^+	g^-	a	g-	86.84	84.20	171.19	-37.39	-785.832802691	3.60
g^+	a	a	g-	83.69	-176.18	173.47	-50.51	-785.836021588	1.58
a	g+	a	a	-177.94	80.97	-172.52	-168.69	-785.831134389	4.64
a	g^+	a	g-	178.67	85.87	174.71	-49.02	-785.836186313	1.47
a	a	g+	g^+	-177.32	176.06	65.92	50.13	-785.837144307	0.87
a	a	a	g+	175.39	177.76	179.89	56.41	-785.833845516	2.94
a	**a**	**a**	**g-**	**177.90**	**-174.47**	**178.47**	**-47.42**	**-785.838535810**	**0.00**
a	a	g-	g^+	179.81	178.53	-62.41	75.42	-785.834879306	2.29
a	a	g-	a	179.97	178.34	-65.51	176.80	-785.834840973	2.32
a	a	g-	g^-	178.78	179.25	-66.90	-68.60	-785.834719233	2.40
a	g-	a	a	-155.99	-105.18	-163.31	-167.56	-785.831784652	4.24
a	g^-	g^-	g^+	179.26	-81.79	-58.53	74.14	-785.833289249	3.29
a	g-	g^-	a	179.66	-82.57	-62.65	175.70	-785.833158489	3.37
a	g^-	g^-	g^-	179.84	-82.40	-61.58	-68.66	-785.832614787	3.72
g^-	a	g+	g^+	-84.52	176.61	68.94	53.44	-785.834927222	2.26
g^-	g^-	a	g-	-74.55	-80.08	-166.17	-58.84	-785.830399507	5.11
g^-	g^-	g^-	g^-	-78.61	-85.32	-64.51	-66.57	-785.828425975	6.34

Table 2:
B3LYP/6-31G(d) optimized parameters for the minima of *R*-Fragment A.

Conformational Assignment				χ_1 (degrees)	χ_2 (degrees)	χ_3 (degrees)	χ_{10} (degrees)	Energy (hartree)	Rel E (Kcal• mol^{-1})
χ_1	χ_2	χ_3	χ_{10}						
g^+	g^+	g^+	g^+	78.66	85.51	64.48	66.64	-785.828425897	6.34
g^+	g^+	a	g^+	74.44	80.27	166.22	58.86	-785.830399472	5.11
g^+	a	g^-	g^-	84.56	-176.64	-68.86	-53.52	-785.834927568	2.26
a	g^+	g^+	g^+	-179.82	82.40	61.44	68.99	-785.832614704	3.72
a	g^+	g^+	a	-179.85	82.74	62.70	-175.60	-785.833159064	3.37
a	g^+	g^+	g^-	-179.33	81.90	58.61	-74.35	-785.833289337	3.29
a	g^+	a	a	156.09	105.16	163.35	167.64	-785.831784831	4.24
a	a	g^+	g^+	-178.82	-179.20	66.89	68.63	-785.834719251	2.40
a	a	g^+	a	179.99	-178.34	65.45	-176.78	-785.834841115	2.32
a	a	g^+	g^-	-179.64	-178.70	62.36	-75.51	-785.834880226	2.29
a	**a**	**a**	**g^+**	**-178.53**	**175.39**	**-178.18**	**47.53**	**-785.838535919**	**0.00**
a	a	a	g^-	-175.20	-177.94	-179.89	-56.46	-785.833846146	2.94
a	a	g^-	g^-	177.68	-176.27	-65.84	-50.64	-785.837142473	0.87
a	g^-	a	g^+	-178.26	-86.25	-174.77	49.15	-785.836187425	1.47
a	g^-	a	a	177.86	-80.88	172.56	168.92	-785.831134398	4.64
g^-	a	a	g^+	-83.67	176.13	-173.69	50.76	-785.836021086	1.58
g^-	g^-	a	g^+	-87.09	-84.22	-171.18	37.39	-785.832806928	3.60
g^-	g^-	a	a	-85.33	-66.15	-179.25	177.98	-785.827602283	6.86
g^-	g^-	g^-	g^-	-71.75	-86.37	-54.09	-60.91	-785.829262278	5.82

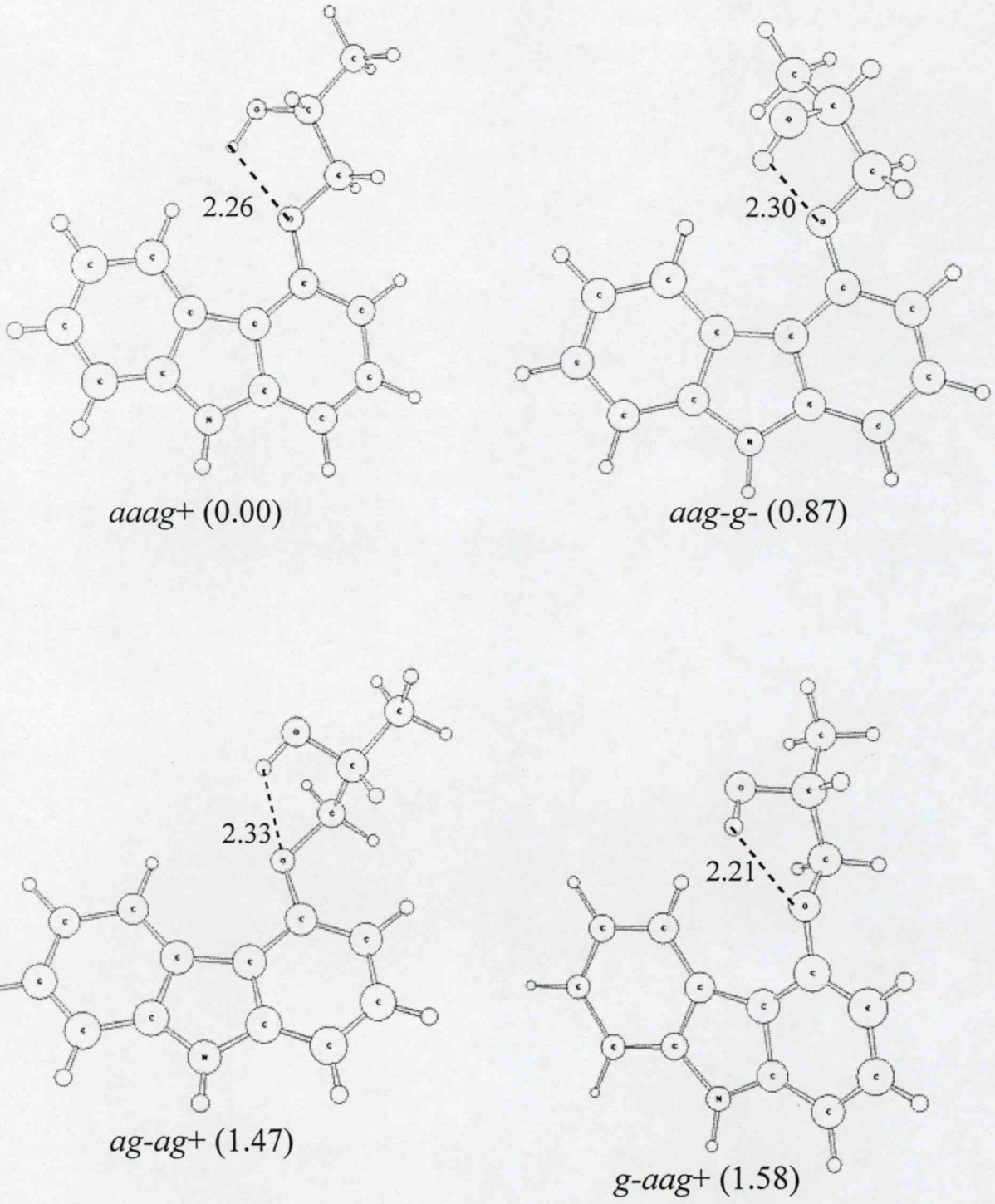

Figure 10: Molecular structures of the four low energy (defined as a conformer relative energy less than two Kcal•mol^{-1}) *R*-Fragment A conformers. Structures were fully optimized at the B3LYP/6-31G(d) level of theory (c.f. **Table 2** for optimized parameters).

5.1.2 Hartree-Fock MDCA of Protonated Fragment B

Optimization of the protonated Fragment B PEHS uncovers a total of 18 converged minima out of a possible 81 (22.2%) (c.f. **Table 3**). The dominant structural characteristic is that all minima possess torsional angle χ_{10} in the *g+* position. With regards to IMAF, low energy structures possess an H-bond between O11 and either of the nitrogen H_S or H_R protons. This H-bond results in the formation of a five-membered ring similar in all conformers to that of global minima *aaag+* (c.f. **Figure 11**). Conformers with this H-bond and five-membered ring motif all have relative energies less than four Kcal•mol^{-1} (*g+ag+g+*, *g+aag+*, *g+ag-g+*, *g+g-ag+*, *g+g-g-g+*, *ag+g+g+*, *ag+ag+*, *ag+g-g+*, *aag+g+*, *aaag+*, *aag-g+*) while all other structures have extended conformations without any IMAF and possess relative energies between six and 13 Kcal•mol^{-1}.

Table 3:
Optimized minima for the PEHS of 2(*S*)-1-(ethylamonium)propane-2-ol (Fragment B) computed at the RHF/3-21G level of theory.

Conformational Assignment				χ_4 (degrees)	χ_5 degrees)	χ_6 (degrees)	χ_{10} (degrees)	Energy (hartree)	Relative Energy (kcal•mol^{-1})
χ_4	χ_5	χ_6	χ_{10}						
g^+	g^+	g^+	g^+	57.38	66.37	58.14	70.70	-324.793727316	7.32
g^+	a	g^+	g^+	77.45	155.53	66.95	66.96	-324.803348723	1.28
g^+	a	a	g^+	77.04	157.33	-179.56	67.45	-324.804338872	0.66
g^+	a	g^-	g^+	77.04	158.06	-75.46	67.12	-324.802468298	1.83
g^+	g^-	a	g^+	89.94	-98.15	179.17	65.87	-324.801304451	2.56
g^+	g^-	g^-	g^+	88.01	-100.37	-75.18	65.30	-324.800033440	3.36
a	g^+	g^+	g^+	160.44	84.73	75.97	51.78	-324.803380654	1.26
a	g^+	a	g^+	159.67	82.59	-178.21	50.43	-324.804820840	0.36
a	g^+	g^-	g^+	151.31	95.77	-64.00	50.51	-324.801332654	2.55
a	a	g^+	g^+	163.82	-160.12	74.88	52.72	-324.803518745	1.17
a	**a**	**a**	**g^+**	**163.43**	**-158.84**	**179.48**	**52.99**	**-324.805389226**	**0.00**
a	a	g^-	g^+	163.01	-157.12	-67.28	53.23	-324.804392810	0.63
a	g^-	g^-	g^+	-175.68	-67.90	-56.89	47.87	-324.794908573	6.58
g^-	a	g^+	g^+	-65.71	179.45	71.69	61.00	-324.785812572	12.28
g^-	a	a	g^+	-65.08	-178.48	-179.82	61.68	-324.787326426	11.33
g^-	a	g^-	g^+	-64.62	-175.20	-70.01	62.22	-324.785836750	12.27
g^-	g^-	a	g^+	-60.25	-69.11	-175.71	65.39	-324.785622305	12.40
g^-	g^-	g^-	g^+	-60.25	-67.59	-67.79	64.38	-324.783970218	13.44

Although only 22% of the possible protonated PEHS minima converged, this value may be revised in light of the *gauche* effect seen at the *g*+ position for torsional angle χ_{10}. When one considers only the 27 conformational minima where χ_{10} is in the *g*+ position, then 66.7% of conformers converged and were found. Contrasting, zero minima converged for conformational assignments where torsional angle χ_{10} was either in the *anti* or *g*- position. This illustrates a dominant *gauche* effect in the conformational identity of Fragment B and perhaps for carvedilol. The Newman projections in **Figure 11** illustrate that the smallest steric hindrance occurs when χ_{10} is in the *g*+ orientation.

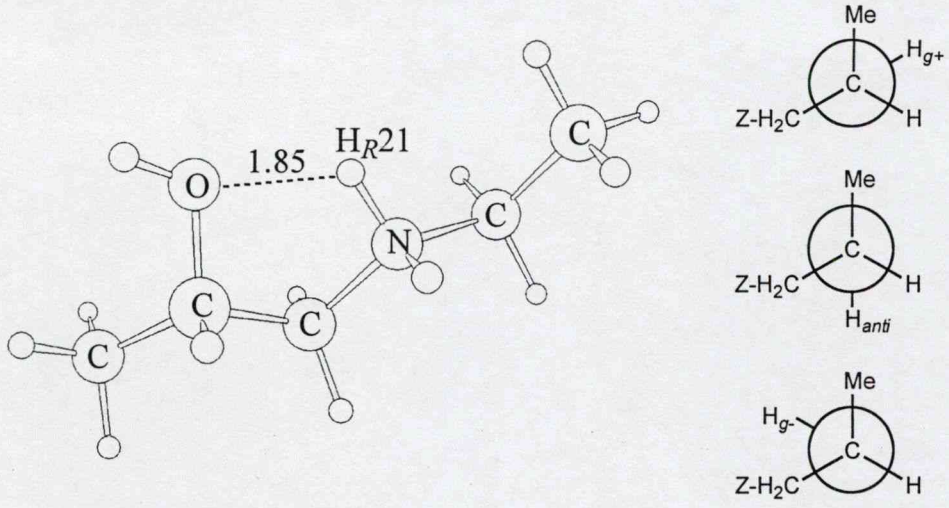

Figure 11: Optimized global minima (conformer *aaag*+) of the protonated Fragment B PEHS (left). All structures with an O11-nitrogen H_S/H_R proton H-bond displayed a similar structure characterized by an intramolecular five-membered ring. Newman projections along the C3-O11 bond (C3 front and O11 rear) display the *g*+, *anti*, and *g*- conformations of torsional angle χ_{10} at the stereocentre of Fragment B and carvedilol (right).

Although conformer relative energies suggest H-bonding acts as the dominant IMAF, it is necessary to note that the χ_{10} torsional angle energetic barrier of rotation (and the corresponding *g*+ *gauche* effect) is perhaps the most dominating influence dictating the conformational identity of Fragment B because the *gauche* effect is seen in all geometrically optimized minima, regardless of H-bonding. Thus, it can be concluded that torsional angle χ_{10} will assume a *g*+ position in carvedilol's side-chain irrespective of IMAF. Low energy conformers, however, would be expected to display H-bonding.

5.1.3 Hartree-Fock MDCA of Protonated Fragment C

MDCA of protonated Fragment C reveals that, instead of the expected 81 conformers, a total of 24 converged minima were found (30% convergence) (c.f. **Table 4**). Out of the 24 converged minima, only 17 were unique conformational assignments, while the remaining seven conformers were variations of three conformational assignments (*g+ag-a*, *aaaa*, and *g-ag+a*) and are denoted with superscripts A, B, C etc. for a given conformation subset (c.f. **Table 4**).

Table 4:
Optimized minima for the PEHS of aminoethoxy-2-methoxy-benzene (Fragment C) at the RHF/3-21G level of theory.

Conformational Assignment				χ_7 (degrees)	χ_8 (degrees)	χ_9 (degrees)	χ_{11} (degrees)	Energy (hartree)	Rel E (kcal• mol^{-1})
χ_7	χ_8	χ_9	χ_{11}						
g^+	**g^+**	**g^+**	**g^-**	**44.46**	**71.68**	**70.76**	**-98.81**	**-549.873068247**	**0.00**
g^+	a	a	a	41.80	122.91	120.56	-179.67	-549.863583899	5.95
g^+	a	g^-	a^A	38.30	-137.12	-115.57	-169.54	-549.872527050	0.34
g^+	a	g^-	a^B	59.99	-140.29	-81.29	156.52	-549.870278796	1.75
g^+	a	g^-	a^C	61.03	-135.10	-77.42	144.54	-549.870234030	1.78
g^+	g^-	a	g^-	95.14	-39.40	135.84	-96.81	-549.861239554	7.42
g^+	g^-	g^-	g^+	62.23	-116.45	-73.64	90.67	-549.871425222	1.03
a	g^+	g^+	g^-	-175.06	102.35	95.80	-95.49	-549.842004194	19.49
a	g^+	a	g^+	-174.20	77.79	-127.36	93.40	-549.837892957	22.07
a	g^+	a	a	-179.37	85.80	-129.12	152.78	-549.837297717	22.45
a	a	a	a^A	-177.24	-120.95	-125.46	170.49	-549.843128026	18.79
a	a	a	a^B	-173.85	-154.80	136.74	-170.71	-549.839012663	21.37
a	a	a	a^C	173.93	154.89	-136.52	170.67	-549.839012786	21.37
a	a	a	a^D	177.21	120.95	125.47	-170.55	-549.843128037	18.79
a	g^-	a	a	178.28	-85.73	129.14	-152.73	-549.837297782	22.45
a	g^-	a	g^-	174.22	-77.75	127.31	-93.33	-549.837893074	22.07
a	g^-	g^-	g^+	174.87	-102.32	-95.66	94.96	-549.842004180	19.49
g^-	g^+	g^+	g^-	-62.22	116.49	73.65	-90.73	-549.871425197	1.03
g^-	g^+	a	g^+	-95.37	38.43	-135.16	96.23	-549.861238102	7.42
g^-	a	g^+	a^A	-60.90	135.26	77.29	-144.62	-549.870235279	1.78
g^-	a	g^+	a^B	-60.10	139.67	80.64	-155.33	-549.870277713	1.75
g^-	a	g^+	a^C	-38.27	137.07	115.59	169.53	-549.872526998	0.34
g^-	a	a	a	-42.04	-122.90	-120.37	179.24	-549.863582322	5.95
g^-	**g^-**	**g^-**	**g^+**	**-44.44**	**-71.70**	**-70.74**	**98.83**	**-549.873068367**	**0.00**

Fragment C conformers are stabilized by internal H-bonding between nitrogen protons (H1, H15, H26) and oxygen atoms (O5 and O12). Strong intramolecular ion-dipole interactions are also present between the protonated positive nitrogen centre and the oxygen atoms. The protonated PEHS global minima, conformer *g+g+g+g-* (and it axis chiral pair *g-g-g-g+*; axis chirality is discussed below in **5.2 Stereochemical Relationships of Carvedilol**), possess an eight-membered ring formed by a short H-bond between H1 and O12 and a longer H-bond between H1 and O5 forming a five-membered ring (c.f. **Figure 12**, left). The bifurcated H-bonding along with both oxygen atoms oriented towards the positive nitrogen confers a very stable conformational motif to Fragment C. The bifurcated H-bond split between both oxygen atoms and forming the eight-membered ring is also the most prevalent structural feature of the protonated Fragment C PEHS; conformers with the lowest relative energies, under two kcal•mol^{-1}, all contain this structural feature.

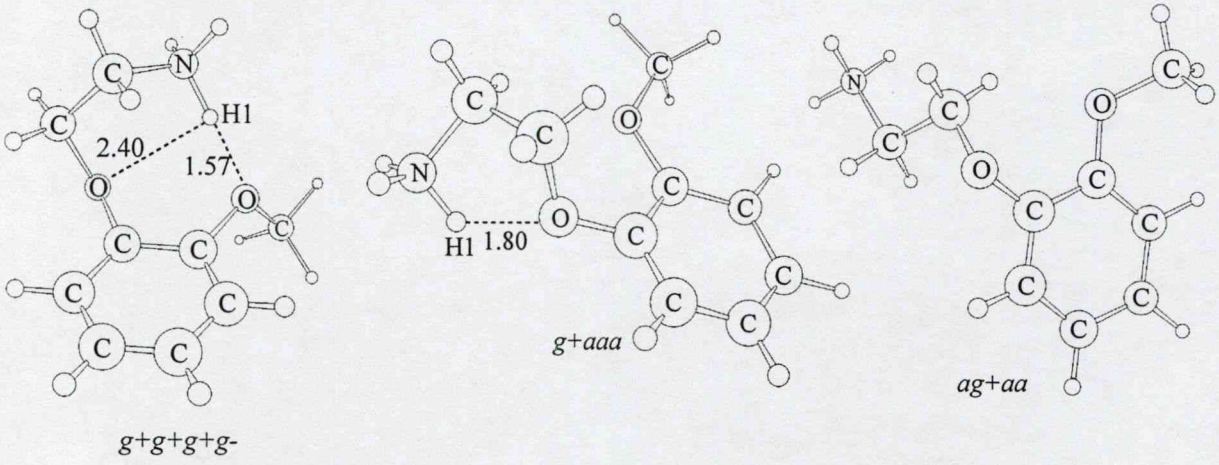

Figure 12: Optimized global minima of the protonated Fragment C PEHS (*g+g+g+g-*) exhibits both a five- and eight-membered ring with a bifurcated H-bond (along with the global minima, all protonated conformers with relative energy less than two kcal•mol^{-1} has this structural feature). Conformer *g+aaa* has a moderate relative energy (5.95 kcal•mol^{-1}) and exhibits a five-membered ring while conformer *ag+aa* had the largest relative energy (22.45 kcal•mol^{-1}) of the protonated PEHS and possesses a fully extended conformation.

Conformers with moderate relative energies possess only one H-bond as opposed to a bifurcated one. Conformers *g+aaa* and *g+g-ag-* (and axis chiral pairs) have relative energies of 5.95 and 7.42 kcal•mol^{-1}, respectively; *g+aaa* contains a 1.80 Å H-bond forming a five-membered ring with O5 (c.f. **Figure 12**, middle) while conformation *g+g-ag-* displays a 1.54 Å H-bond forming an eight-membered ring with O12. The latter eight-membered was similar to that seen in the global minima except that O5 was not involved in any other H-bonding. Finally, structures with torsional angle χ_7 oriented in the *anti* position have the side-chain positioned away from the ring, and therefore, are not able to form any internal H-bonds. The disparity in the relative energies of these conformers, about 20 kcal•mol^{-1}, indicates of their lack of IMAF. Conformer *ag+aa* possess the largest relative energy of the PEHS (c.f. **Figure 12**, right).

As stated above, the Fragment C PEHS contains a number of different converged structures within a respective conformational assignment. Although the majority of subset conformers are very similar to each other, conformer *g+ag-a*^{A} and *g+ag-a*^{B} converged to very different geometries. The former conformer is the only structure with two different protons involved in two distinct H-bonds forming separate five- and eight-membered rings (c.f. **Figure 13**, left). Conformer *g+ag-a*^{B} and *g+ag-a*^{C} possess the more prevalent bifurcated H-bond structural feature (c.f. **Figure 6**, middle and right).

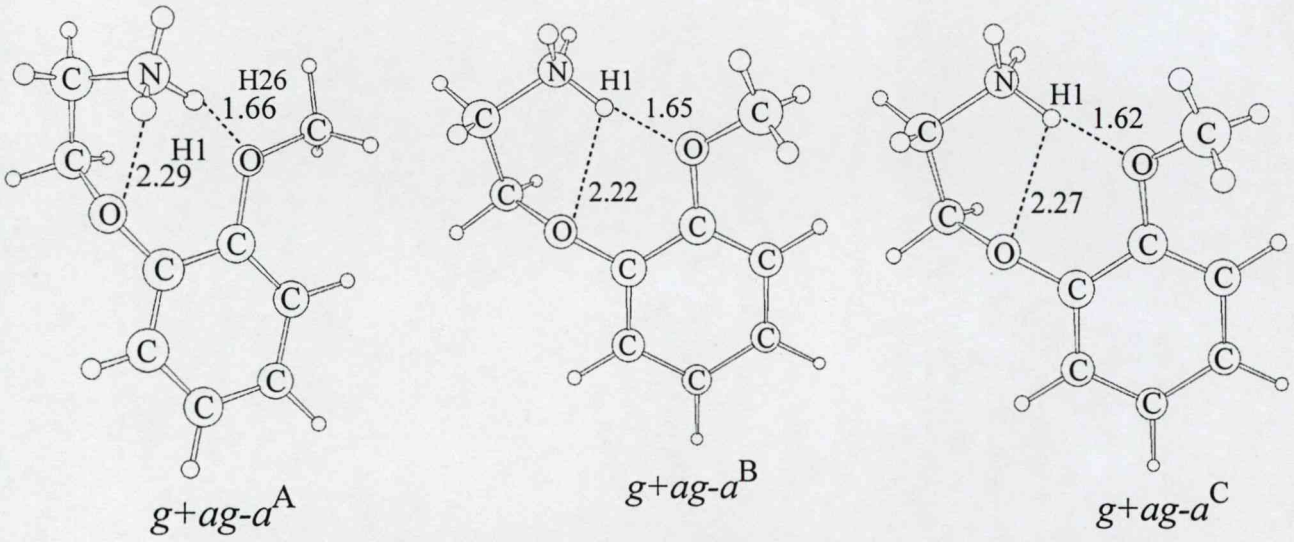

Figure 13: Converged minima of the protonated Fragment C PEHS *g+ag-a* subset: *g+ag-a*^{A} (0.34 kcal•mol^{-1}), *g+ag-a*^{B} (1.75 kcal•mol^{-1}), and *g+ag-a*^{C} (1.78 kcal•mol^{-1}).

5.2 Stereochemical Relationships of Carvedilol

5.2.1 Chiral Parameters of Fragment A & Selected Analogues

All analogue structures presented in **Figure 7** were subject to the same RHF/3-21G (data not shown), RHF/6-31G(d) (data not shown), and B3LYP/6-31G(d) optimization methods described above for *S*- and *R*-Fragment A. The converged minima of the pro-chiral non-carbazole analogues IV-H_2 (c.f. **Table 5**) and IV-Me_2 (c.f. **Table 6**) reveal the presence of axis chirality. Hence, although these structures will not rotate plane-polarized light, they possess axis chirality which occurs when the structures adopt conformations with asymmetric electron density planes. Irrespective of the presence of four different substituents (point chirality), the chirality induced by an asymmetric distribution of electron density (axis chirality) is always present whenever the structure adopts asymmetric conformations. Further, like enantiomers of point chirality, axis chiral conformers come in pairs. The only exception to this is the *aaa* conformation because it possesses a symmetric electron density plane, and therefore, axis chirality is not present. However, all other conformations are paired according to equation **[21]** which states; for a pro-chiral structure with two energetically equivalent minima, plus (P) and minus (M), all torsional angles for those minima are switched from clockwise (CW) to counter-clockwise (CCW) rotation.

$$E_P = E_M \qquad [21]$$
$$f_P(\chi_2, \chi_3, \chi_{10}) = f_M(-\chi_2, -\chi_3, -\chi_{10}).$$

Conformational analysis of III-[H,Me]-*S* (c.f. **Table 7**) and III-[H,Me]-*R* (c.f. **Table 8**) displays both point and axis chirality. Consequently, enantiomeric pairs require not only the switching of point chirality from the *R*- to *S*-stereoisomer but also the switching of all torsional angles from CW to CCW rotation due to axis chirality in asymmetric conformations (c.f. equation **[22]**). Corollary to the latter, it can be reviewed that all *S*- and *R*-Fragment A converged minima (c.f. **Table 3** and **4**) also possess the combination of point and axis chirality and can be described by equation **[22]**. In these enantiomeric systems, all minima must have energetically equivalent enantiomers while all other pairs have diastereomeric relationships.

$$E_R = E_S \qquad [22]$$
$$f_R(\chi_1, \chi_2, \chi_3, \chi_{10}) = f_S(-\chi_1, -\chi_2, -\chi_3, -\chi_{10}).$$

Table 5:
B3LYP/6-31G(d) optimized minima for the PEHS of IV-H_2.

Conformational Assignment			χ_2 (degrees)	χ_3 (degrees)	χ_{10} (degrees)	Energy (hartree)	Rel E (kcal• mol^{-1})
χ_2	χ_3	χ_{10}					
g^+	g^+	a	74.84	64.71	-176.35	-269.542422374	5.34
g^+	g^+	g^-	84.22	55.17	-43.31	-269.548526782	1.51
g^+	a	g^+	82.10	176.20	67.87	-269.543841268	4.45
g^+	a	a	83.07	178.41	-177.30	-269.543541796	4.63
g^+	a	g^-	81.30	178.57	-67.44	-269.544279753	4.17
g^+	g^-	a	81.32	-75.42	173.05	-269.545157695	3.62
g^+	g^-	g^-	78.24	-71.37	-63.90	-269.545185796	3.60
a	g^+	g^+	-178.77	64.47	58.69	-269.544928112	3.76
a	**g^+**	**g^-**	**-173.81**	**59.60**	**-49.85**	**-269.550927094**	**0.00**
a	a	g^+	-178.30	179.68	69.45	-269.546263161	2.93
a	a	a	180.00	180.00	180.00	-269.545824036	3.20
a	a	g^-	178.30	-179.67	-69.48	-269.546263144	2.93
a	**g^-**	**g^+**	**173.81**	**-59.60**	**49.85**	**-269.550927095**	**0.00**
a	g^-	g^-	178.77	-64.47	-58.69	-269.544928111	3.76
g^-	g^+	g^+	-78.24	71.37	63.90	-269.545185796	3.60
g^-	g^+	a	-81.32	75.42	-173.04	-269.545157695	3.62
g^-	a	g^+	-81.30	-178.57	67.44	-269.544279753	4.17
g^-	a	a	-83.07	-178.41	177.30	-269.543541796	4.63
g^-	a	g^-	-82.10	-176.20	-67.87	-269.543841268	4.45
g^-	g^-	g^+	-84.23	-55.18	43.31	-269.548526783	1.51
g^-	g^-	a	-74.84	-64.71	176.35	-269.542422374	5.34

Table 6:
B3LYP/6-31G(d) optimized minima for the PEHS of IV-Me_2.

Conformational Assignment			χ_2 (degrees)	χ_3 (degrees)	χ_{10} (degrees)	Energy (hartree)	Rel E (kcal• mol^{-1})
χ_2	χ_3	χ_{10}					
g^+	g^-	a	86.21	-71.30	174.64	-348.182592886	3.36
g^+	g^-	g^-	81.08	-67.14	-63.97	-348.182032926	3.71
a	g^+	a	-177.62	69.32	-174.14	-348.181677861	3.94
a	**g^+**	**g^-**	**-174.24**	**55.90**	**-46.46**	**-348.187950829**	**0.00**
a	a	g^+	-178.29	179.67	70.72	-348.184592291	2.11
a	a	a	180.00	-179.98	-179.95	-348.184521481	2.15
a	a	g^-	178.29	-179.67	-70.72	-348.184592292	2.11
a	**g^-**	**g^+**	**174.24**	**-55.90**	**46.46**	**-348.187950829**	**0.00**
a	g^-	a	177.62	-69.32	174.15	-348.181677884	3.94
g^-	g^+	g^+	-81.08	67.13	63.97	-348.182032924	3.71
g^-	g^+	a	-86.20	71.30	-174.64	-348.182592888	3.36

Table 7:
B3LYP/6-31G(d) optimized minima for the PEHS of III-[H,Me]-*S*.

Conformational Assignment			χ_2 (degrees)	χ_3 (degrees)	χ_{10} (degrees)	Energy (hartree)	Rel E (kcal• mol^{-1})
χ_2	χ_3	χ_{10}					
g^+	g^+	a	77.95	63.78	-176.82	-308.861759588	5.58
g^+	g^+	g^-	84.85	52.21	-39.81	-308.868518645	1.33
g^+	g^-	a	83.72	-74.52	175.99	-308.864709683	3.72
g^+	g^-	g^-	79.25	-71.11	-59.35	-308.864078627	4.12
a	g^+	a	-175.69	71.27	-171.49	-308.863878357	4.25
a	**g^+**	**g^-**	**-174.20**	**56.59**	**-45.91**	**-308.870644238**	**0.00**
a	a	g^+	-178.25	174.71	72.56	-308.866380432	2.68
a	a	a	179.74	174.65	177.60	-308.866211574	2.78
a	a	g^-	179.01	176.00	-66.05	-308.866106215	2.85
a	g^-	g^+	174.72	-58.47	48.62	-308.869488916	0.72
a	g^-	a	177.81	-72.18	174.53	-308.863889500	4.24
g^-	g^+	g^+	-79.71	68.49	66.38	-308.864165391	4.07
g^-	g^+	a	-83.12	73.27	-173.44	-308.864450066	3.89
g^-	a	g^+	-81.44	176.91	70.61	-308.864404100	3.92
g^-	a	a	-83.98	176.50	175.83	-308.864066200	4.13
g^-	a	g^-	-80.81	179.85	-63.76	-308.863793580	4.30

Table 8:
B3LYP/6-31G(d) optimized minima for the PEHS of III-[H,Me]-*R*.

Conformational Assignment			χ_2 (degrees)	χ_3 (degrees)	χ_{10} (degrees)	Energy (hartree)	Rel E (kcal• mol^{-1})
χ_2	χ_3	χ_{10}					
g^+	a	g^+	80.81	-179.85	63.76	-308.863793580	4.30
g^+	a	a	83.98	-176.50	-175.83	-308.864066200	4.13
g^+	a	g^-	81.44	-176.91	-70.61	-308.864404100	3.92
g^+	g^-	a	83.12	-73.27	173.44	-308.864450067	3.89
g^+	g^-	g^-	79.71	-68.49	-66.38	-308.864165391	4.07
a	g^+	a	-177.81	72.18	-174.53	-308.863889500	4.24
a	g^+	g^-	-174.72	58.47	-48.62	-308.869488917	0.72
a	a	g^+	-179.01	-176.00	66.05	-308.866106219	2.85
a	a	a	-179.73	-174.65	-177.60	-308.866211567	2.78
a	a	g^-	178.26	-174.71	-72.56	-308.866380447	2.68
a	**g^-**	**g^+**	**174.20**	**-56.59**	**45.91**	**-308.870644238**	**0.00**
a	g^-	a	175.69	-71.27	171.50	-308.863878355	4.25
g^-	g^+	g^+	-79.25	71.11	59.35	-308.864078622	4.12
g^-	g^+	a	-83.72	74.52	-175.99	-308.864709683	3.72
g^-	g^-	g^+	-84.85	-52.21	39.81	-308.868518645	1.33
g^-	g^-	a	-77.95	-63.78	176.82	-308.861759588	5.58

5.2.2 Extrapolation of Chiral Parameters to Carvedilol & Fragments

The above discussion illustrates that the properties of achiral and chiral structures are not completely distinct, given that the only differences occur at the chiral centre, and that deductions about particular stereoisomers and achiral systems can be made without having to undergo full exhaustive MDCA processes. The utility of these principles is that the presence of axis and point chirality ensures that not all conformations will be unique but rather can be predicted from stereochemical relationships as those described in equation **[21]** and **[22]**. In light of this, it is evident that the PEHS of Fragment C (c.f. **Table 6**) displays axis chirality and can accordingly be described by equation **[23]**. Furthermore, the minima of *S*-Fragment B can be used to predict the PEHS of *R*-Fragment B with equation **[24]** as Fragment B is a system with both point and axis chirality.

$$E_P = E_M \qquad [23]$$
$$f_P(\chi_7, \chi_8, \chi_9, \chi_{11}) = f_M(-\chi_7, -\chi_8, -\chi_9, -\chi_{11})$$

$$E_S = E_R \qquad [24]$$
$$f_S(\chi_4, \chi_5, \chi_6, \chi_{10}) = f_R(-\chi_4, -\chi_5, -\chi_6, -\chi_{10})$$

Similarly, extrapolating to carvedilol, since it possess a point chiral strereocentre and axis chirality will be present in all asymmetric conformations, all carvedilol minima will occur in analogous pairs as portrayed in equation **[25]**. The outcome of this relationship is that carvedilol can be treated as a molecular system where all results obtained for one stereoisomer can be readily applied to the other. As such, the *R*-carvedilol analysis presented in this dissertation can be promptly applied to *S*-carvedilol as all enantiomeric minima will be paired up according to equation **[25]**. Optimized parameters for a converged minima of *R*-carvedilol require the switching of point chirality from the *R*- to *S*-stereoisomer followed by the switching of optimized torsional angle geometries from CW to CCW rotation.

$$E_R = E_S \qquad [25]$$
$$f_R(\text{index of } \chi_1 \text{ to } \chi_{11}) = f_S(\text{index of } -\chi_1 \text{ to } -\chi_{11})$$

5.3 Multiple Proton Conformational Basicity Calculations

5.3.1 Hartree-Fock Conformational Basicity of Fragment B

Once the protonated PEHS of Fragment B was computed, protons H_S and H_R were abstracted as shown in **Figure 8**. $\Delta E_{vert}(S)$ and $\Delta E_{vert}(R)$ values reveal variable deprotonation energies depending on whether or not one of the protons is involved in internal H-bonding (c.f. **Table 9**). Energies of deprotonation for protons H_S and H_R are comparable for conformers with no H-bonding (usually less that than one Kcal•mol^{-1} difference) while H-bonded protons require an additional six to eight Kcal•mol^{-1} for deprotonation (c.f. **Table 9**). This latter trend is displayed in **Figure 14** (left) indicating that, depending on proton H-bonding, conformers will display differences in energies of deprotonation.

As anticipated, geometry optimization of the deprotonated conformers reduces the majority of differences between the H_S and H_R protons (c.f. **Table 9**). Nonetheless, the H_R proton of conformers *aag+g+* and *aaag+* require an additional 6.05 and 5.79 kcal•mol^{-1}, respectively, for deprotonation compared to the H_S proton (c.f. **Figure 14**, middle) due to the presence of the five-membered ring motif shown in **Figure 11**. Several H_S deprotonated (*g+ag+g+*, *g+aag+*, *ag+g+g+*, *ag+ag+*, *ag+g-g+*) and H_R deprotonated (*g+g-ag+* and *g+g-g-g+*) conformers have $\Delta\Delta E$ values greater than 15 Kcal•mol^{-1} (c.f. **Table 9**) suggesting the initial deprotonated structures are high energy and significant stability is conferred upon optimization; i.e., if the proton abstracted is involved in IMAF, then the $\Delta\Delta E$ values are larger because a major geometry rearrangement is necessary. This is opposed to the deprotonation of protons not involved in IMAF which do not require any significant alterations in geometry (c.f. **Figure 14**, right).

The overall trend indicates that conformers devoid of IMAF have lower energies of deprotonation; as relative energy increased, ΔE_{vert} and ΔE_{opt} values decreased. Further, H-bonding creates an antagonistic behaviour between protons because if the H_S proton is involved in H-bonding, then the H_R proton is easily deprotonated and *vice versa*. Graphically, the latter is displayed as mirror-like increases and decreases in energies of deprotonation for different protons in H-bonded conformers (c.f. conformations 2-12 in **Figure 14**, left). This data suggests a direct dependence of multiple proton basicity on conformation as different protons will be favoured depending on the conformation, and subsequent IMAF, adopted.

Table 9:
Summary of the energies of deprotonation and their respective differences for the H_S (H16) and H_R (H21) deprotonation of converged protonated Fragment B conformers at the RHF/3-21G level of theory. Superscript numbers in the χ_4 Protonated Conformation column are used as labels for conformations in **Figure 14**.

Protonated Conformation				$\Delta E_{vert}(S)$ (Kcal• mol^{-1})	$\Delta E_{vert}(R)$ (Kcal• mol^{-1})	$\lvert\Delta E_{vert}(S) - \Delta E_{vert}(R)\rvert$ (Kcal• mol^{-1})	$\Delta E_{opt}(S)$ (Kcal• mol^{-1})	$\Delta E_{opt}(R)$ (Kcal• mol^{-1})	$\lvert\Delta E_{opt}(S) - \Delta E_{opt}(R)\rvert$ (Kcal• mol^{-1})	$\Delta\Delta E(S)$ (Kcal• mol^{-1})	$\Delta\Delta E(R)$ (Kcal• mol^{-1})	$\lvert\Delta\Delta E(S) - \Delta\Delta E(R)\rvert$ (Kcal• mol^{-1})
χ_4	χ_5	χ_6	χ_{10}									
$^{1}g^+$	g^+	g^+	g^+	257.65	258.41	0.76	250.56	252.14	1.58	7.09	6.27	0.82
$^{2}g^+$	a	g^+	g^+	271.67	264.25	7.42	256.60	255.47	1.13	15.07	8.78	6.29
$^{3}g^+$	a	a	g^+	272.05	264.05	8.00	256.92	255.36	1.56	15.13	8.69	6.44
$^{4}g^+$	a	g^-	g^+	271.76	263.62	8.14	257.24	254.82	2.42	14.52	8.80	5.72
$^{5}g^+$	g^-	a	g^+	266.43	273.26	6.83	257.05	253.46	3.59	9.38	19.80	10.42
$^{6}g^+$	g^-	g^-	g^+	266.15	272.57	6.42	256.76	253.29	3.47	9.39	19.28	9.89
^{7}a	g^+	g^+	g^+	271.77	265.24	6.53	255.78	257.02	1.24	15.99	8.22	7.77
^{8}a	g^+	a	g^+	272.11	265.31	6.80	256.06	257.13	1.07	16.05	8.18	7.87
^{9}a	g^+	g^-	g^+	272.92	265.37	7.55	254.60	256.64	2.04	18.32	8.73	9.59
^{10}a	a	g^+	g^+	264.10	271.66	7.56	255.87	261.92	6.05	8.23	9.74	1.51
^{11}a	a	a	g^+	264.61	272.01	7.40	256.42	262.21	5.79	8.19	9.8	1.61
^{12}a	a	g^-	g^+	264.79	271.66	6.87	256.52	257.96	1.44	8.27	13.7	5.43
^{13}a	g^-	g^-	g^+	258.87	258.59	0.28	252.86	252.01	0.85	6.01	6.58	0.57
$^{14}g^-$	a	g^+	g^+	251.81	253.10	1.29	245.51	246.69	1.18	6.30	6.41	0.11
$^{15}g^-$	a	a	g^+	252.34	253.07	0.73	246.17	247.28	1.11	6.17	5.79	0.38
$^{16}g^-$	a	g^-	g^+	252.41	252.42	0.01	246.13	246.48	0.35	6.28	5.94	0.34
$^{17}g^-$	g-	a	g^+	252.41	251.95	0.46	246.45	245.20	1.25	5.96	6.75	0.79
$^{18}g^-$	g^-	g^-	g^+	252.42	251.57	0.85	246.42	244.58	1.84	6.00	6.99	0.99

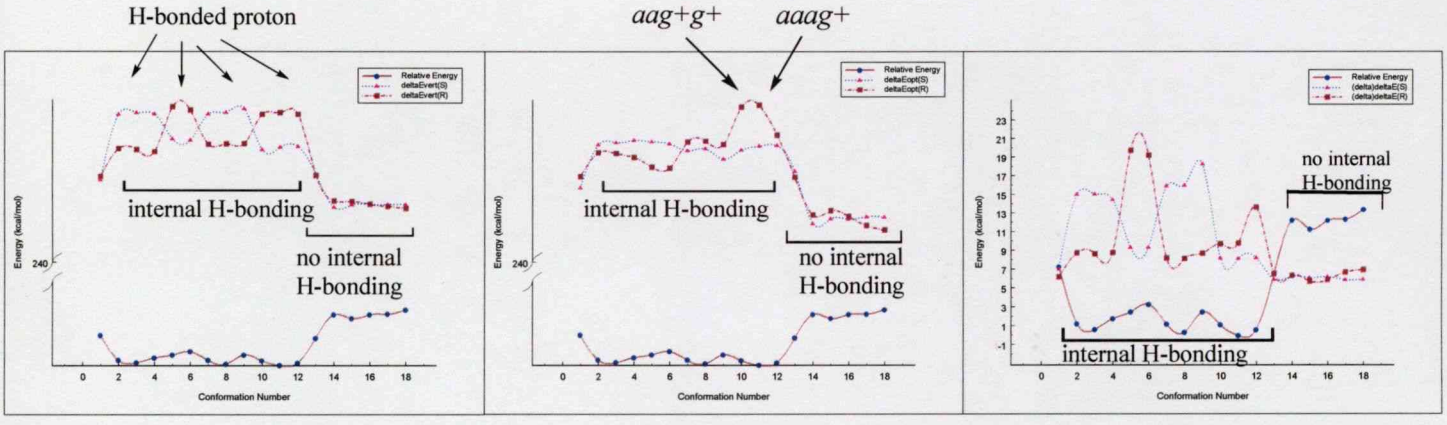

Figure 14: Trends in $\Delta E_{vert}(S)$ and $\Delta E_{vert}(R)$ (left), $\Delta E_{opt}(S)$ and $\Delta E_{opt}(R)$ (middle), $\Delta\Delta E(S)$ and $\Delta\Delta E(R)$ (right) as compared to the conformer relative energy of converged Fragment B minima. Conformation Number labels are defined with superscripts in the χ_4 Protonated Conformation column of **Table 11**.

5.3.2 Hartree-Fock Conformational Basicity of Fragment C

The converged minima of the protonated Fragment C PEHS were independently deprotonated of H_a, H_{g+}, and H_{g-} protons (c.f. **Table 10**). Vertical energies of deprotonation show the greatest difference when H-bonded protons are abstracted; protons involved in H-bonding require on average an additional 5-10 Kcal•mol^{-1}. Contrasting, high relative energy structures (conformations with torsional angle χ_7 in the *anti* position and no IMAF) have energies of deprotonation 25-35 Kcal•mol^{-1} lower than that of low relative energy conformers. Although large variation is found in energies of deprotonation (with regards to the three protons) for the same conformation in H-bonded conformers, high relative energy conformers all possess comparable energies for all three protons due to the lack of any H-bonding.

Table 10:
Summary of the energies of deprotonation for each converged conformation of protonated Fragment C at the RHF/3-21G level of theory.

Protonated Conformation				$\Delta E_{vert}(a)$ (Kcal• mol^{-1})	$\Delta E_{opt}(a)$ (Kcal• mol^{-1})	$\Delta\Delta E(a)$ (Kcal• mol^{-1})	$\Delta E_{vert}(g+)$ (Kcal• mol^{-1})	$\Delta E_{opt}(g+)$ (Kcal• mol^{-1})	$\Delta\Delta E(g+)$ (Kcal• mol^{-1})	$\Delta E_{vert}(g-)$ (Kcal• mol^{-1})	$\Delta E_{opt}(g-)$ (Kcal• mol^{-1})	$\Delta\Delta E(g-)$ (Kcal• mol^{-1})
χ_7	χ_8	χ_9	χ_{11}									
g^+	g^+	g^+	g^-	280.43	261.69	18.74	270.32	258.26	12.06	270.54	257.89	12.65
g^+	a	a	a	263.54	254.76	8.78	264.01	254.90	9.11	269.55	254.90	14.65
g^+	a	g^-	a^A	276.07	259.87	16.20	271.49	259.87	11.62	277.51	259.83	17.68
g^+	a	g^-	a^B	278.99	264.29	14.70	268.01	258.46	9.55	269.12	258.41	10.71
g^+	a	g^-	a^C	279.45	264.29	15.16	268.18	258.43	9.75	269.52	258.39	11.13
g^+	g^-	a	g^-	266.12	250.47	15.65	273.09	254.38	18.71	267.07	253.55	13.52
g^+	g^-	g^-	g^+	278.66	257.26	21.40	268.18	257.06	11.12	269.22	257.26	11.96
a	g^+	g^+	g^-	248.61	240.76	7.85	247.69	241.21	6.48	248.76	240.73	8.03
a	g^+	a	g^+	244.97	238.34	6.63	244.49	238.18	6.31	243.73	238.35	5.38
a	g^+	a	a	245.43	239.81	5.62	245.39	239.92	5.47	244.49	239.95	4.54
a	a	a	a^A	248.70	242.73	5.97	247.81	242.89	4.92	248.90	242.88	6.02
a	a	a	a^B	245.33	240.55	4.78	246.04	240.38	5.66	245.85	240.29	5.56
a	a	a	a^C	245.84	240.29	5.55	246.03	240.38	5.65	245.32	240.55	4.77
a	a	a	a^D	246.31	240.30	6.01	245.23	240.30	4.93	246.12	240.14	5.98
a	g^-	a	a	245.44	239.81	5.63	244.50	239.95	4.55	245.39	239.92	5.47
a	g^-	a	g^-	244.97	238.34	6.63	243.73	238.35	5.38	244.49	238.18	6.31
a	g^-	g^-	g^+	248.73	240.73	8.00	247.67	241.21	6.46	248.57	240.76	7.81
g^-	g^+	g^+	g^-	278.68	257.26	21.42	269.24	257.26	11.98	268.20	257.06	11.14
g^-	g^+	a	g^+	273.12	254.38	18.74	266.08	250.47	15.61	267.03	253.55	13.48
g^-	a	g^+	a^A	279.47	264.27	15.20	269.54	258.39	11.15	268.20	258.43	9.77
g^-	a	g^+	a^B	279.05	264.27	14.78	269.16	258.41	10.75	268.01	258.46	9.55
g^-	a	g^+	a^C	277.50	259.83	17.67	271.48	259.87	11.61	276.07	259.87	16.20
g^-	a	a	a	269.50	254.90	14.60	263.94	254.90	9.04	263.48	254.75	8.73
g^-	g^-	g^-	g^+	280.43	261.69	18.74	270.54	257.89	12.65	270.32	258.26	12.06

Geometry optimizations reduce most of the energies of deprotonation, however, conformations with internal stabilization still require significantly more energy (20-30 Kcal•mol^{-1}) for deprotonation (c.f. **Table 10**). Respective $\Delta\Delta E$ values are typically large (8-21 kcal•mol^{-1}) for conformers with IMAF while conformers with no IMAF have $\Delta\Delta E$ values of less than eight Kcal•mol^{-1}. The latter indicates that high relative energy conformers provide ideal structures for deprotonation as they do not require major geometrical changes to rearrange into local minima. Like the secondary amine Fragment B, the primary amine Fragment C illustrates a major dependence of multiple proton basicity on protonated conformation and IMAF.

5.3.3 Extrapolating Conformational Basicity Observations to Carvedilol

Previous work on carvedilol has revealed energies of deprotonation of 234 and 238 Kcal•mol^{-1} for only two conformations, irrespective of the protons deprotonated, at the RHF/6-31G(d) level of theory[11]. Fragment B and C possess energies of deprotonation ranging from 245 to 262 and 238 to 264 Kcal•mol^{-1}, respectively, disclosed *via* full optimization of their particular PEHS minima at the RHF/3-21G level of theory. These fragment values are directly comparable to carvedilol but with a greater number of conformations surveyed and finer selectivity with regards to proton abstraction. It can so be concluded that Fragment B, and to an extent Fragment C, successfully modeled the basic side-chain of carvedilol.

Extrapolating to carvedilol, it is expected that structural and energetic parameters of proton abstraction pathways will vary depending on the molecular conformation of the protonated structure. In carvedilol's uncoupling of oxidative phosphorylation in mitochondria, differences in energies of deprotonation have been previously attributed to uncharacterized effects of conformation[11]. In light of the Fragment B and C conformational basicity results presented, it is likely that these conformational factors are related to the dependence of multiple proton basicity on conformation; this is to say, certain protonated conformations of carvedilol will bias protons differently, and therefore, have different energies of deprotonation. Thus, for carvedilol, and other protonated molecular systems, it is expected that molecular conformation and intrinsic structural motifs will predetermine, at least with regards to energetics, the type of protonophoretic mechanisms most utilized or favoured by enzymes and substrates in proton shuttling pathways.

5.4 Predicting & Optimizing Selected Conformations of Carvedilol

5.4.1 Predicting Carvedilol Conformers Using Individual Fragment Results

Converged low energy (defined as possessing a conformer relative energy ≤ 2.00 Kcal•mol^{-1}) Fragment A, B, and C conformations were utilized in an attempt to predict corresponding significantly populated conformers of carvedilol. The fragment structures fitting this criterion and used for prediction are as follows, *R*-Fragment A: *aaag+*, *aag-g-*, *ag-ag+*, *g-aag+* (c.f. **Table 2**); *S*-Fragment B: *aaag+*, *ag+ag+*, *aag-g+*, *g+aag+*, *aag+g+*, *ag+g+g+*, *g+ag+g+*, *g+ag-g+* (c.f. **Table 3**); Fragment C: *g+g+g+g-*, *g-g-g-g+*, *g+ag-a*, *g-ag+a*, *g+g-g-g+*, *g-g+g+g-*, (c.f. **Table 4**). These conformations were combined to create a comprehensive list of 240 *R*-carvedilol conformers (list not shown) hypothesized to be low energy states of the carvedilol PEHS. Converged fragment conformational assignments were permutated so that the 240 conformational predictions constitute a maximum, distinct and non-redundant list. Conformations are labeled from C-*R*-1 to C-*R*-240 for tabulation purposes.

The only incidence of overlapping, non-symmetrical torsional angles between the three fragments is torsional angle χ_{10} in Fragment A and B; however, these only differ in their χ_{10} orientation in one conformation. Consequently, carvedilol predictions all possess torsional angle χ_{10} in the *g+* position except for those combinations involving Fragment A conformation *aag-g-* which have resulting conformational predictions with torsional angle χ_{10} in the both the *g+* and *g-* positions. The combinations for *R*-carvedilol with torsional angle χ_{10} in the *g+* and *g-* position are displayed in equation **[26]** and **[27]**, respectively. The total number of 240 unique conformations is summed by: equation **[26]** (χ_{10} = *g+*) + equation **[27]** (χ_{10} = *g-*) = 192 (χ_{10} = *g+*) + 48 (χ_{10} = *g-*) = 240.

(4 Fragment A conformations) x (8 Fragment B conformations) x (6 Fragment C conformations) = 192 *R*-carvedilol unique conformations (All possess torsional angle χ_{10} in the *g+* position.) **[26]**

(1 Fragment A conformation) x (8 Fragment B conformations) x (6 Fragment C conformations) = 48 *R*-carvedilol unique conformations (All possess torsional angle χ_{10} in the *g-* position.) **[27]**

5.4.2 Hartree-Fock Optimization of Carvedilol Conformational Predictions

All 240 carvedilol input (i.e., predicted) structures were optimized at the RHF/3-21G level of theory. Consequently, a total of 121 unique carvedilol conformations were revealed with a range in relative conformer energy of ~23 Kcal•mol^{-1} (data not shown). However, not all of the 121 converged conformations were predicted from the fragment analysis; 35 novel conformations became apparent upon optimization (labeled as conformers C-*R*-241 to C-*R*-275). Thus, there is an absolute convergence of 44% (121/275) for all conformers evaluated. Overall, the carvedilol PEHS displays dramatic conformational flexibility with conformations converging at various points of the PEHS.

In order to arrive at a set of Hartree-Fock optimized low energy conformers for the carvedilol PEHS, all converged conformations are plotted according to their respective relative energy (c.f. **Figure 15**). The plot illustrates the inherent flexibility of the carvedilol molecule as converged conformations are dispersed over a large range of relative energies. However, there is a definitive set of nine low energy conformations in the bottom right-hand corner of **Figure 15**; these conformations are bounded by a conformer relative energy of less than four Kcal•mol^{-1} and are clearly divided from the rest of the converged structures. These nine conformations, C-*R*-246 to C-*R*-251, C-*R*-258, C-*R*-272, C-*R*-273, were selected for gas and solvent phase optimization with high level DFT calculations.

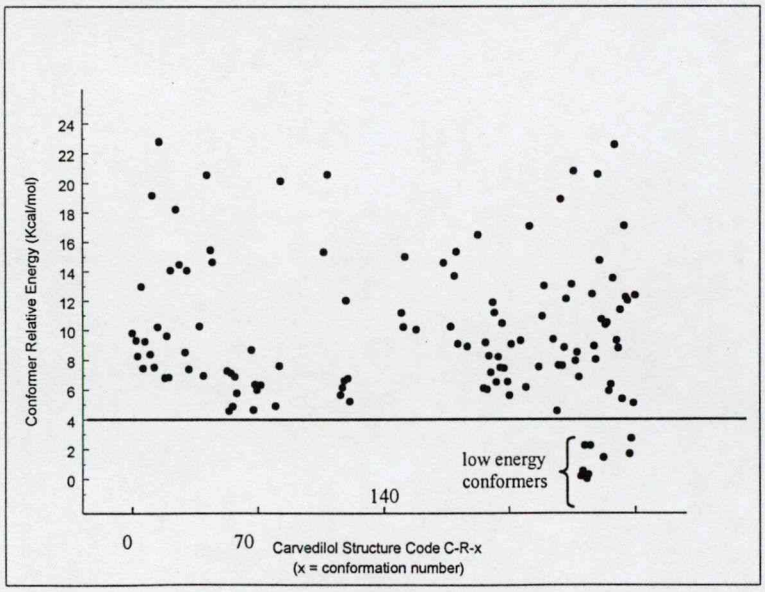

Figure 15: Graphical representation of the conformer relative energies for all RHF/3-21G converged carvedilol structures.

5.4.3 Density Functional Optimization of Low Energy Carvedilol States

5.4.3.1 Density Functional Gas Phase Optimizations

According to equation **[5]**, a summary of optimized conformation for all nine converged structures of carvedilol is presented in **Table 11**. Upon gas phase DFT optimization, all nine conformations exhibit a gas phase relative energy of less than two Kcal•mol^{-1} (c.f. **Table 12**) compared with a conformer relative energy of less than four Kcal•mol^{-1} for the RHF/3-21G structures (c.f. **Figure 15**).

Table 11:
Optimized torsional angle orientations of carvedilol low energy structures. Molecular conformation is displayed as [gas phase RHF/3-21G/gas phase B3LYP/6-31G(d)/DMSO solvent phase B3LYP/6-31G(d)/water solvent phase B3LYP/6-31G(d)]. (Explicit values of torsional angles are found in **Tables 12-14**.)

Structure Code	Torsional Angle Conformation										
	χ_1	χ_2	χ_3	χ_4	χ_5	χ_6	χ_7	χ_8	χ_9	χ_{10}	χ_{11}
C-*R*-246	[g+/a/ a/a]	[a/a/ a/a]	[g-/g-/ g-/g-]	[g+/g+/ g+/g+]	[g+/g+/ g+/g+]	[a/a/ a/a]	[g-/g-/ g-/g-]	[g-/g-/ g-/g-]	[g-/g-/ g-/g-]	[g+/g+/ g+/g+]	[g+/g+/ g+/g+]
C-*R*-247	[g+/g+/ g+/g+]	[a/a/ a/a]	[g-/g-/ g-/g-]	[g+/g+/ g+/g+]	[g+/g+/ g+/g+]	[g+/g+/ g+/g+]	[g-/g-/ g-/g-]	[a/a/ a/a]	[g+/g+/ g+/g+]	[g+/g+/ g+/g+]	[a/a/ a/a]
C-*R*-248	[g+/g+/ g+/g+]	[a/a/ a/a]	[g-/g-/ g-/g-]	[g+/g+/ g+/g+]	[a/a/ a/a]	[a/a/ a/a]	[g+/g+/ g+/g+]	[a/a/ a/a]	[g-/g-/ g-/g-]	[g+/g+/ g+/g+]	[g+/g+/ g+/g+]
C-*R*-249	[g+/g+/ g+/g+]	[a/a/ a/a]	[g-/g-/ g-/g-]	[g+/g+/ g+/g+]	[a/a/ a/a]	[g-/g-/ g-/g-]	[g-/g-/ g-/g-]	[g-/g-/ g-/g-]	[g-/g-/ g-/g-]	[g+/g+/ g+/g+]	[g+/g+/ g+/g+]
C-*R*-250	[g+/g+/ g+/g+]	[a/a/ a/a]	[g-/g-/ g-/g-]	[g+/g+/ g+/g+]	[a/a/ a/a]	[g-/g-/ a/a]	[g+/g+/ g+/g+]	[a/a/ a/a]	[g-/g-/ g-/g-]	[g+/g+/ g+/g+]	[a/a/ a/a]
C-*R*-251	[g+/g+/ g+/g+]	[a/a/ a/a]	[g-/g-/ g-/g-]	[g+/g+/ g+/g+]	[a/a/ a/a]	[g-/g-/ g-/g-]	[g-/g-/ g-/g-]	[a/a/ a/a]	[g+/g+/ g+/g+]	[g+/g+/ g+/g+]	[a/a/ a/a]
C-*R*-258	[g+/g+/ g+/g+]	[a/a/ a/a]	[g-/g-/ g-/g-]	[g+/g+/ g+/g+]	[g+/g+/ g+/g+]	[a/a/ a/a]	[g-/g-/ g-/g-]	[g+/g+/ g+/g+]	[g+/g+/ g+/g+]	[g+/g+/ g+/g+]	[g-/g-/ g-/g-]
C-*R*-272	[g+/g+/ g+/g+]	[a/a/ a/a]	[g-/g-/ g-/g-]	[g+/g+/ g+/g+]	[g+/g+/ g+/g+]	[g+/g+/ g+/g+]	[g+/g+/ g+/g+]	[g+/g+/ g+/g+]	[g+/g+/ g+/g+]	[g+/g+/ g+/g+]	[g-/g- /g-/g-]
C-*R*-273	[g+/g+/ g+/g+]	[a/a/ a/a]	[g-/g-/ g-/g-]	[g+/g+/ g+/g+]	[a/a/ a/a]	[g+/g+/ g+/g+]	[g+/g+/ g+/g+]	[a/a/ a/a]	[g-/g-/ g-/g-]	[g+/g+/ g+/g+]	[a/a/ a/a]

Table 12:
Gas phase ($\varepsilon = 0.0$) optimized values and energies for the converged conformers of the protonated *R*-carvedilol surface at the B3LYP/6-31G(d) level of theory.

Structure Code	Torsional Angle (degrees)											Energy (Hartree)	Relative Energy (Kcal• mol^{-1})
	χ_1	χ_2	χ_3	χ_4	χ_5	χ_6	χ_7	χ_8	χ_9	χ_{10}	χ_{11}		
C-*R*-246	147.66	-178.59	-61.82	67.01	92.56	179.24	-47.81	-68.16	-68.34	54.30	90.60	-1340. 99055043	0.11
C-*R*-247	107.44	-171.16	-53.41	67.92	85.46	108.38	-51.47	146.95	106.47	56.63	177.53	-1340. 98911556	1.01
C-*R*-248	100.13	-169.42	-51.87	67.66	-167.27	-168.85	65.24	-129.63	-77.61	49.02	106.78	-1340. 98917601	0.98
C-*R*-249	98.69	-171.84	-51.36	71.22	-162.18	-59.94	-47.41	-71.17	-70.95	51.53	96.98	-1340. 99072989	0.00
C-*R*-250	97.94	-174.38	-51.60	71.66	-170.02	-108.22	51.08	-145.73	-113.20	61.69	178.99	-1340. 99052227	0.13
C-*R*-251	97.63	-172.97	-49.97	72.69	-173.97	-66.19	-46.46	175.94	112.05	55.44	179.71	-1340. 98883102	1.19
C-*R*-258	97.47	-174.15	-55.86	63.28	83.88	175.26	-60.45	116.50	69.38	57.43	-88.53	-1340. 98857046	1.36
C-*R*-272	92.99	-175.06	-54.27	63.77	80.27	63.58	44.88	71.86	68.43	57.95	-94.63	-1340. 98826529	1.55
C-*R*-273	91.74	-177.88	-52.41	72.27	171.03	63.65	47.12	-177.41	-110.11	51.57	-177.05	-1340. 98879141	1.22

Close scrutiny of the DFT low energy conformations reveals that seven (C-*R*-246 to C-*R*-250, C-*R*-258, and C-*R*-272) of the nine conformations possess a novel tetra-centric spiro-type structural motif. The tetra-centric conformation is flanked on one side by the 13-membered aromatic carbazole ring (centre 1) which is connected to a six-membered ring closed *via* an intramolecular O···H-N H-bond between the carbazole ether oxygen and a proton of the positive nitrogen centre (ring **a**; centre 2). The same protonated secondary nitrogen atom – *via* the other proton – forms an eight-membered ring (ring **b**; centre 3) through another intramolecular O···H-N H-bond to the methoxy oxygen of carvedilol. The "right side" of the carvedilol conformation if flanked by the di-substituted benzene ring (centre 4) which also forms part of ring **b**. Rings **a** and **b** are formed *via* short H-bonds that are in all cases less than two Angstroms in length and always involves both protons of the nitrogen centre (c.f. **Figure 16**). In order that this tetra-centric structural motif form, it is necessary that the protonated nitrogen centre is present for the concomitant formation of the two essential O···H-N H-bonds. If only one proton (in the neutral amine form) is present, instead of the positive protonated centre, it is likely that it would not be possible to form rings **a** and **b**.

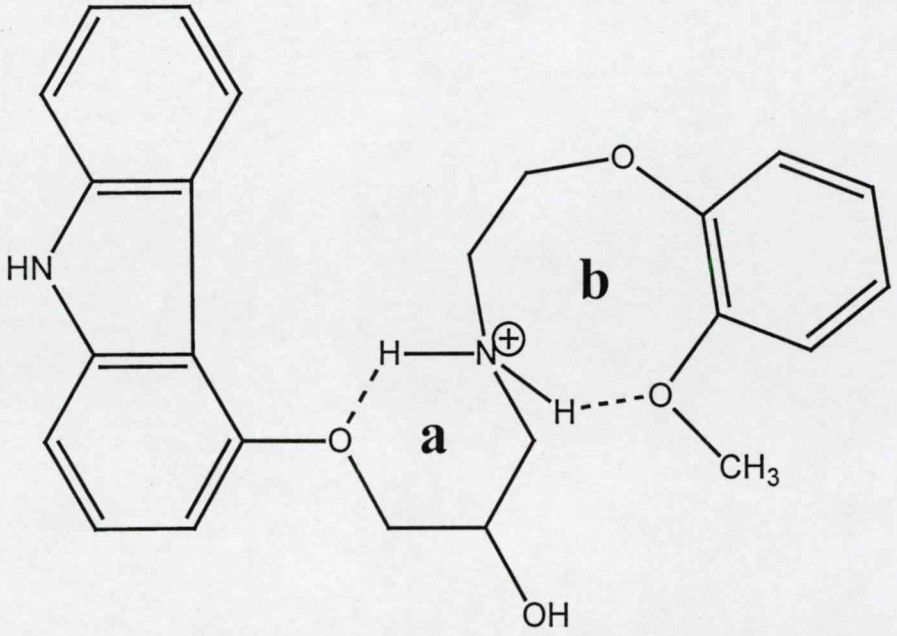

Figure 16: Schematic representation of the "tetra-centric" spiro-type conformational motif exhibited by most carvedilol low energy conformations. This structural motif consists of a six-membered ring (ring **a**) bonded to the carbazole centroid and an eight-membered ring (ring **b**) bonded to the substituted benzene. Note that the rings are not co-planar but distorted and juxtaposed as shown in **Figure 17**.

The global minima, conformer C-*R*-249, is shown in **Figure 17** (top). Conformations C-*R*-251 (c.f. **Figure 17** bottom) and C-*R*-273 do not form any IMAF with the methoxy oxygen (O36), and thus, do not form ring **b**. Aside from differences related to the tetra-centric conformational motif, the nine low energy carvedilol structures can be divided into two groups: those with three internal H-bonds (C-*R*-246, C-*R*-247, C-*R*-251, C-*R*-258, C-*R*-272, and C-*R*-273) and those with four internal H-bonds (C-*R*-248, C-*R*-249, and C-*R*-250). These additional H-bonds form various intramolecular five-membered rings.

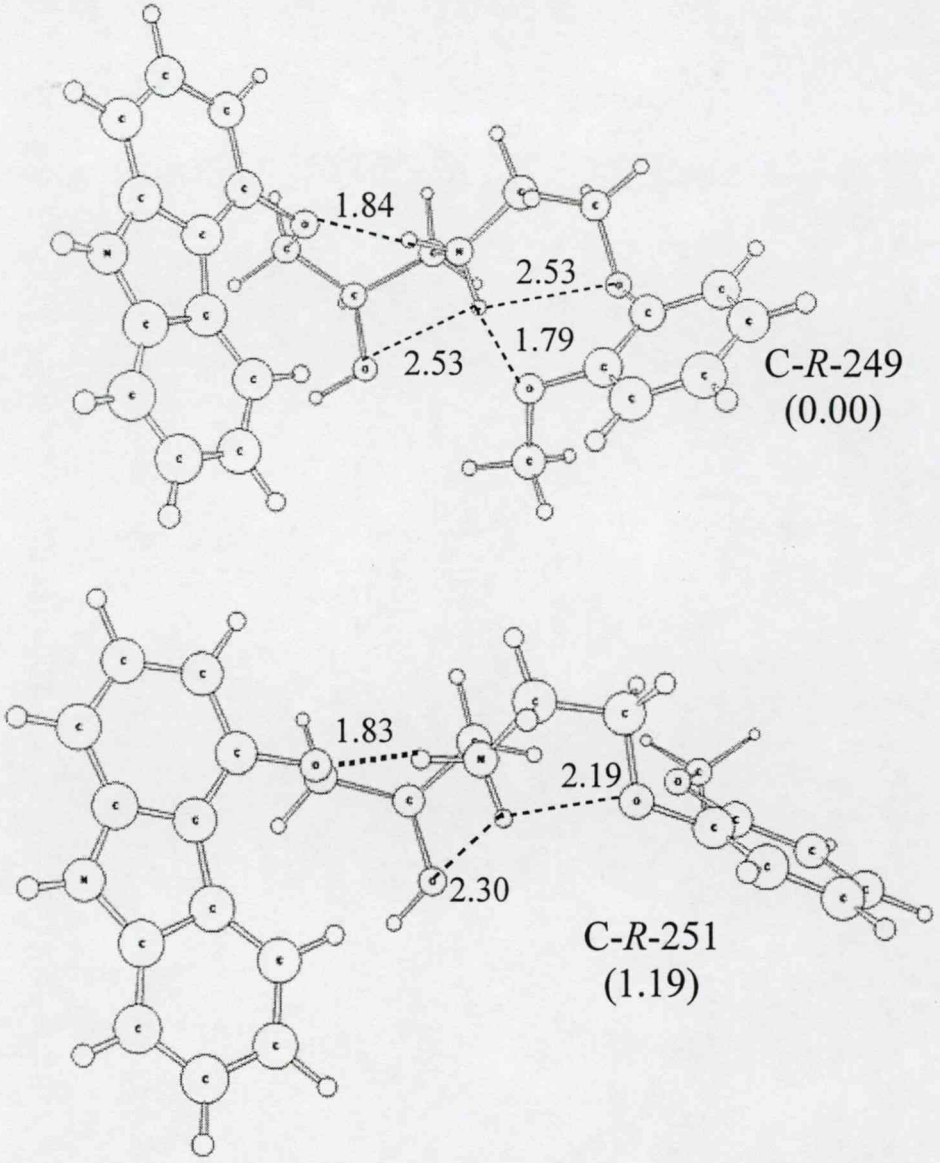

Figure 17: Molecular structures (and relative energies) of conformers C-*R*-249 and C-*R*-251 optimized in the gas phase at the B3LYP/6-31G(d) level of theory (c.f. **Table 12** for optimized parameters). Carvedilol atom numbering is displayed in **Figure 6**.

The rational molecular fragmentation of protonated carvedilol is based on the deconstruction of carvedilol into three dominant pharmacophore fragments: a positive secondary amine side-chain (Fragment B) flanked by an electron-withdrawing group (EWG) carbazole ring system (Fragment A) and an EWG benzene centroid (Fragment C). Given these three structure-activity considerations, it can be rationalized that the prevalence of the tetra-centric conformation in seven of the nine DFT optimized conformers is a result of stabilizing the positive nitrogen centre. The electronic structure of this motif allows the electron-donating groups (EDG) found on the carbazole (ether oxygen bridge, O1) and benzene (methoxy oxygen, O36) rings to act as EDG to their respective centroids, and also to the positive nitrogen centre. The formation of intramolecular rings **a** and **b** facilitates an electron density redistribution process whereby the ether (O1) and methoxy (O36) EDG induct electron density into the positive nitrogen centre *via* O···H-N H-bonds.

Given the above, it can be concluded that although the tetra-centric structural motif represents the preferred and likely most populated gas phase conformation of carvedilol, the nitrogen side-chain can be stabilized by various H-bonds that all serve the function of inducting (or redistributing) electron density into the positive centre. In total, the carvedilol intramolecular H-bond networks are composed of various H-bonds that can originate from two amine proton H-bond donors (H46 and H57) to four oxygen H-bond acceptors (O1, O29, O36, and O41).

The chemical literature available is limited with regards to the detailed description of carvedilol's gas phase structure; thus, it is difficult to compare the above DFT results with previous experimental works. The X-ray diffraction crystal structure of carvedilol, developed by Chen and coworker[60], utilizes the deprotonated neutral form of carvedilol and displays a pair of carvedilol enantiomers interacting *via* short intermolecular O41-H42···N26 H-bonds (two H-bonds per enantiomer pair). However, since the crystal displays neutral intermolecular enantiomer structure, it does not elucidate any intramolecular structural parameters of single-molecule protonated carvedilol. The *bona fide* structural analysis of single-molecule carvedilol performed here is relevant to carvedilol's mechanisms of action because these are a result of one *R*- or *S*-configuration molecule interacting with adrenoceptors, ROS, or Aβ peptides. As such, these single-molecule conformations of carvedilol describe the dominant structures it assumes before any solvent effect occurs and prior to complexing with such molecular targets.

5.4.3.2 Density Functional DMSO & Water Optimizations

DFT optimized gas phase geometries of carvedilol's nine low energy conformers were used as input files for DFT optimization in aprotic DMSO (c.f. **Table 13**) and protic water (c.f. **Table 14**) to bring to light carvedilol's solvent effect. A graphical representation of this solvent effect is displayed in **Figure 18**.

Table 13:
DMSO optimized values and energies for the converged conformers of the protonated *R*-carvedilol surface.

Structure Code	Torsional Angle (degrees)											Energy (Hartree)	Relative Energy (Kcal• mol^{-1})
	χ_1	χ_2	χ_3	χ_4	χ_5	χ_6	χ_7	χ_8	χ_9	χ_{10}	χ_{11}		
C-*R*-246	150.88	179.18	-63.08	67.55	92.89	-179.91	-48.08	-68.00	-69.15	60.25	92.98	-1340. 99216696	1.30
C-*R*-247	108.63	-171.72	-55.13	66.64	84.64	108.06	-51.95	146.85	106.26	58.67	178.65	-1340. 98974697	2.82
C-*R*-248	101.74	-171.19	-54.11	66.06	-172.30	-172.33	63.79	-126.92	-74.53	56.40	98.42	-1340. 99185150	1.50
C-*R*-249	102.46	-172.21	-53.76	69.78	-162.90	-61.65	-47.65	-70.57	-69.72	54.54	92.88	-1340. 99258309	1.04
C-*R*-250	**91.13**	**-175.76**	**-51.32**	**73.87**	**177.54**	**-166.65**	**52.18**	**-162.59**	**-111.58**	**67.08**	**-176.93**	**-1340. 99423903**	**0.00**
C-*R*-251	104.99	-172.30	-52.94	71.61	-175.19	-71.24	-46.43	174.18	113.01	58.03	177.65	-1340. 99089225	2.10
C-*R*-258	115.34	-174.34	-57.00	66.15	87.38	178.29	-60.89	114.39	70.11	65.18	-88.62	-1340. 99075953	2.18
C-*R*-272	96.58	-175.49	-55.15	63.87	80.29	64.83	44.94	71.61	68.40	62.88	-94.46	-1340. 98960067	2.91
C-*R*-273	98.22	177.38	-52.43	74.93	170.96	68.11	48.42	-177.80	-108.48	65.23	-172.71	-1340. 99194603	1.44

Table 14:
Water optimized values and energies for the converged conformers of the protonated *R*-carvedilol surface.

Structure Code	Torsional Angle (degrees)											Energy (Hartree)	Relative Energy (Kcal• mol^{-1})
	χ_1	χ_2	χ_3	χ_4	χ_5	χ_6	χ_7	χ_8	χ_9	χ_{10}	χ_{11}		
C-*R*-246	150.84	179.18	-63.08	67.55	92.88	-179.87	-48.08	-68.01	-69.16	60.35	93.04	-1340. 99219535	1.32
C-*R*-247	108.23	-171.74	-55.21	66.48	84.80	107.04	-51.55	146.70	106.37	58.30	178.53	-1340. 98976077	2.85
C-*R*-248	101.82	-171.19	-53.92	66.10	-172.10	-171.98	63.68	-126.97	-74.48	56.51	98.38	-1340. 99190386	1.50
C-*R*-249	102.19	-172.53	-53.48	69.90	-163.21	-62.04	-47.86	-70.22	-69.67	56.39	92.20	-1340. 99261927	1.06
C-*R*-250	**91.26**	**-175.77**	**-51.35**	**73.87**	**177.49**	**-166.72**	**52.19**	**-162.67**	**-111.57**	**67.18**	**-176.89**	**-1340. 99430184**	**0.00**
C-*R*-251	105.11	-172.31	-52.99	71.60	-175.21	-71.30	-46.43	174.16	113.05	58.12	177.61	-1340. 99093123	2.12
C-*R*-258	114.80	-174.65	-57.11	66.04	86.98	178.26	-60.87	114.42	70.10	65.88	-88.43	-1340. 99081121	2.19
C-*R*-272	96.56	-175.39	-55.28	63.90	80.69	64.73	44.89	71.69	68.43	62.40	-94.42	-1340. 98962465	2.93
C-*R*-273	98.46	177.28	-52.58	74.95	170.94	68.52	48.46	-177.73	-108.50	65.62	-172.58	-1340. 99200916	1.44

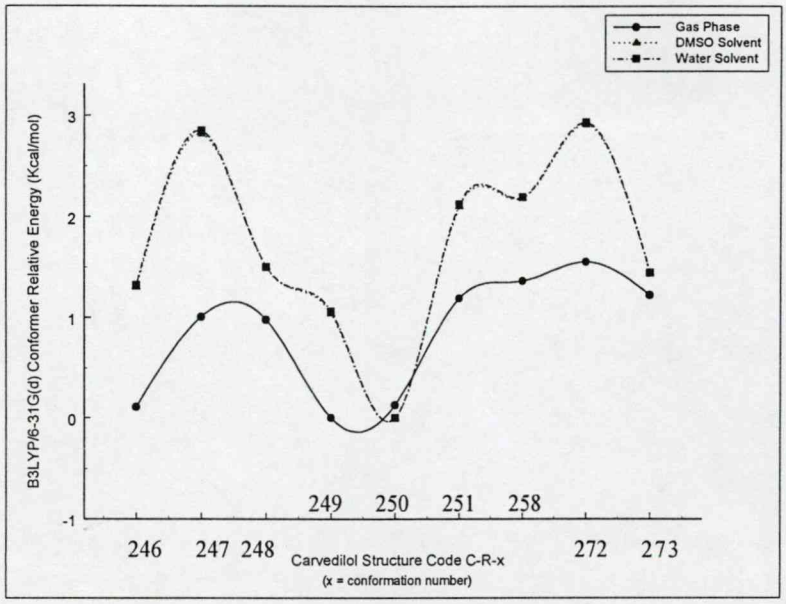

Figure 18: Graphical representation of the solvent effect of carvedilol. Gas, DMSO, and water phase relative energies are presented for all carvedilol structures optimized. Note that the DMSO and water relative energies extensively overlap each other.

Superficially from **Figure 18**, it is evident that DMSO and water solvation of carvedilol produces the same effect on relative energy. Pertaining to electronic structure, torsional angle conformation distribution in **Table 11** indicates that, for a given carvedilol conformer, torsional angle orientation is consistent between RHF and DFT optimizations as well as between gas, DMSO, and water phase calculations. This suggests carvedilol's low energy states have significant conformational transition state energy barriers that prevent major re-arrangements and interconversions between states in the solvent phase.

In comparing gas, DMSO, and water converged conformers, the only conformer that underwent any significant structural changes is C-*R*-250 (c.f. **Figure 19**) in rotating torsional angle χ_6 from the *g-* position (RHF and DFT gas phase results; c.f. **Table 11** and **12**) to the *anti* position (DFT DMSO and water calculations; c.f. **Table 13** and **14**). This conformer re-arranged such that the methoxy oxygen (O36) no longer interacts with any amine protons, and therefore, cannot form ring **b** pertaining to the tetra-centric structure. In the solvent phases, C-*R*-250 still possesses a short O1···H46-N H-bond but formed a much stronger O41···H57···O29 bifurcated H-bond with a distance of 2.27 Å and 2.15 Å, respectively, in both DMSO and water (c.f. **Figure 19**).

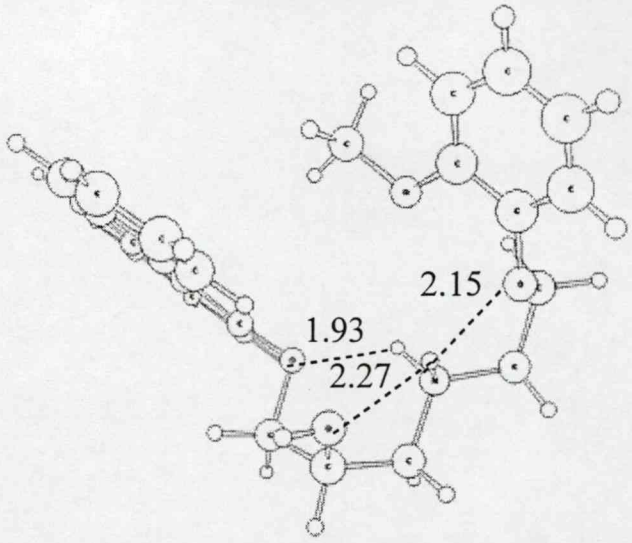

Figure 19: Molecular structure of the DMSO and water solvent global minima, conformer C-*R*-250, optimized at B3LYP/6-31G(d).

Given the DFT solvent calculations, carvedilol can be said to have a subtle solvent effect with regards to energetics and electronic structure. On the whole, most structures preferred the tetra-centric motif seen in the gas phase suggesting there is significant conformational transition state energy barriers that affects the interconversion rates between the different conformational states. It can thus be stated that the carvedilol gas phase conformations are excellent starting points for any structural or mechanistic analysis of carvedilol.

5.4.4 Theoretical Resolution of Carvedilol's Conformational Surface

All torsional angle orientations necessary for carvedilol to assume the tetra-centric motif and low energy states presented in **Tables 12**, **13**, and **14** are expressed in equation **[28]**. Although the carvedilol PEHS is one of large conformational flexibility, there is unanticipated rigidity in four (χ_2, χ_3, χ_4, χ_{10}) of the 11 torsional angles as these only assume one orientation. Further, torsional angle χ_1 assumes an *anti* conformation in only one conformer (C-*R*-246) while *g*+ in all other converged carvedilol structures. Hence, it can be proposed that it is the large carbazole-containing pharmacophore that dictates the prevalent conformations of carvedilol. Likewise, a dominant *gauche* effect exists in torsional angle χ_{10} of carvedilol.

$$\begin{array}{ll} \chi_1 = g+/a & \chi_6 = g+/a/g- \\ \chi_2 = a & \chi_7 = g+/g- \\ \chi_3 = g- & \chi_8 = g+/a/g- \\ \chi_4 = g+ & \chi_9 = g+/g- \\ \chi_5 = g+/a & \chi_{10} = g+ \\ & \chi_{11} = g+/a/g- \end{array} \qquad \textbf{[28]}$$

5.5 NMR Spectroscopy of Carvedilol in DMSO Solvent

Carvedilol NMR chemical shifts and assignments are presented in **Table 15**. Initially, a ROESY spectrum was utilized to analyze the rigid structure of carvedilol about torsional angles χ_1, χ_2, χ_3, χ_4, and χ_5. The ROESY spectrum shows carbazole proton H22 gives good intensity cross peaks to non-equivalent H39 and H40 protons indicating H22 is close to these two protons and there is rigid motion about torsional angles χ_1, χ_2, and χ_3. Moreover, ROESY spectra also indicates the H44 and H45 protons are not equivalent, and as a result, rotation about torsional angles χ_4 and χ_5 is likely hindered. Given these results, along with the fact that DMSO solvent generally destroys weak intramolecular H-bonding, the ROESY spectrum suggests that: (1) the Fragment A associated torsional angles of carvedilol are indeed inflexible, and (2) the intramolecular H-bond networks present in the carvedilol structure are strong and persistent.

Table 15
NMR proton chemical shifts and assignments for carvedilol in DMSO (§ indicates NMR shifts cross-checked with reference **73**).

Proton Chemical Shift (θ, ppm)	**Proton Assignment**	**Relevant Section of Carvedilol**
8.27	H15§	Carbazole Aromatic Ring
7.14	H16§	
7.35	H17§	
7.46	H18§	
11.26	H19	
7.1	H20§	
7.3	H21§	
6.7	H22§	
5.2	H42	Stereocentre
4.19	H43	
4.15	H39§ & H40§	Connecting Backbone
2.88	H44	
2.83	H45	
2.95	H47 & H48	
4.01	H49§ & H50§	
3.73	H38, H55, & H56	Methoxy Group
Unresolved ~ 6.8-6.9	H51, H52, H53, & H54	Aromatic Benzene Ring

With reference to the DFT DMSO optimized structures, all conformers possess at least one intramolecular H-bond involving an amine proton and the carbazole ether oxygen (O1) which will severely hinder rotation involving torsional angles χ_1, χ_2, χ_3, χ_4, and χ_5 (c.f. **Figure 19**). In addition, because the nitrogen centre is protonated and interacts *via* H-bond formation with O29 and O36 in low energy states, further hindrance is placed on the rotation of these five torsional angles. As such, the ROESY spectra substantiates the DFT structures in that, given the various intramolecular H-bonds that carvedilol forms, it would be expected that protons H39 and H40 as well as H44 and H45 constitute non-equivalent centres.

Scalar coupling of protons H44 and H45 (C25 centre) to proton H43 (stereocentre C24) was analyzed to closely inspect the behaviour of torsional angle χ_4. Scalar coupling data with integration of NOE intensity curves reveals a large J-coupling value and corresponding large NOE intensity for proton H45 to proton H43 suggesting a dihedral value of ± 60 degrees (c.f. **Figure 20**, left). Meanwhile, low J-coupling and low NOE values were observed for proton H44 to proton H43 implying a dihedral shift of 120 degrees (c.f. **Figure 20**, right).

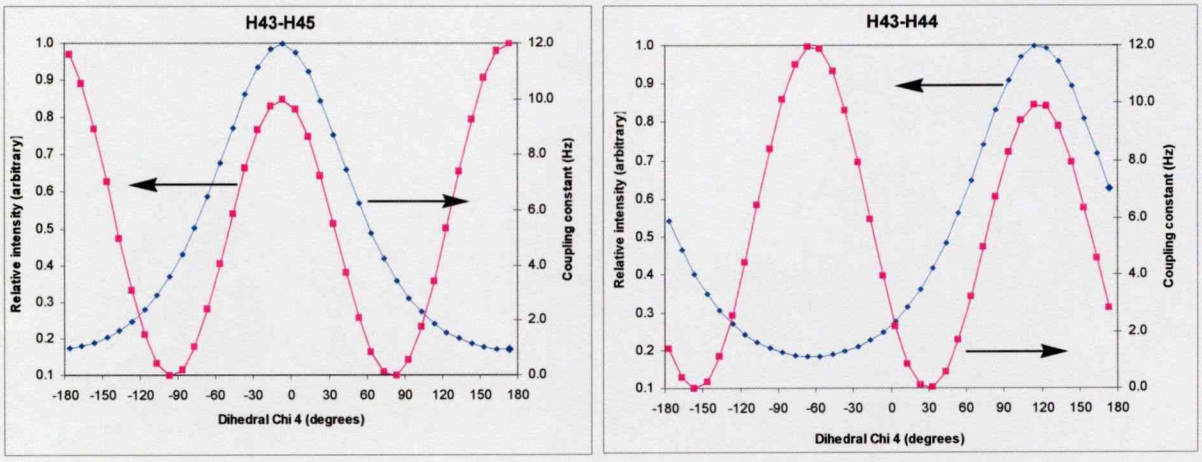

Figure 20: Graphical representation of the relationship between J-coupling and NOE intensity for protons H45 (left) and H44 (right) to stereocentre proton H43.

DMSO optimized carvedilol conformers and their respective optimized parameters (c.f. **Table 13**) reveal that all low energy carvedilol structures have torsional angle χ_4 in the *g*+ orientation; the Newman projection in **Figure 21** displays the *g*+ orientation of torsional angle χ_4. In this *gauche* conformation, proton H45 imparts a large NOE and J-coupling influence to stereocentre proton H43 while proton H44 is shifted relative to torsional angle χ_4. Together, this conformation corroborates the NMR spectroscopy data.

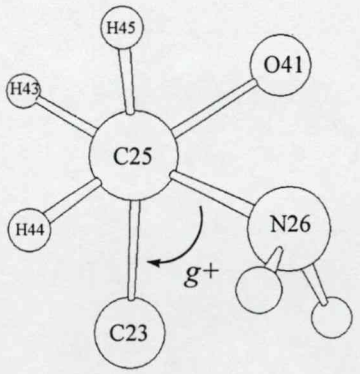

Figure 21: Newman projection of the *g*+ orientation for torsional angle χ_4 of carvedilol found in all gas phase, DMSO, and water optimized structures (c.f. **Tables 12**, **13**, and **14**).

The overlap signal and lack of NMR spectroscopic resolution concerning the aromatic benzene protons (H51, H52, H53, and H54) did not allow for any clear conclusions concerning the Fragment C portion of the carvedilol structure. Overall, the NMR spectroscopy results closely mirror the optimized DFT structures and give full credibility to such high level gas and solvent phase calculations. Furthermore, as a whole, the theoretically- and experimentally-determined carvedilol structures are in extensive agreement and portray carvedilol as a relatively inflexible molecule with various robust IMAF. Hence, carvedilol does not seem to be susceptible to a large solvent effect as its conformers are largely unchanged from gas to solvent phases.

5.6 Evaluation of the Rational Molecular Fragmentation Method

As stated above, given the current cost of computer power and the fact that carvedilol's PEHS possesses an exorbitant number of conformational possibilities (3^{11}), traditional MDCA approaches are daunting and unfeasible. In reality, the problem of solving carvedilol's PEHS is analogous to the difficulties encountered in deciphering complete conformational profiles for molecular system such as drugs and proteins. For carvedilol, this problem has been solved by creating a method in which carvedilol is divided into three molecular fragments, according to pharmacophore structure-activity (c.f. **Figure 4**), and each fragment studied to form predictions before the carvedilol PEHS itself is investigated and optimized.

For assessment of this molecular fragmentation approach, carvedilol predictions (c.f. **5.4.1 Predicting Carvedilol Conformers Using Individual Fragment Results**) and optimized parameters (since no appreciable solvent effect is observed for carvedilol, gas phase DFT structures are used; c.f. **Table 12**) are compared with regards to torsional angle conformation distribution (c.f. **Table 16**).

Table 16
Summary of conformation distribution for carvedilol and Fragments A, B, and C. Dominant torsional angle conformation for carvedilol and corresponding fragment conformation is bolded for ease of comparison. ‡Conformation distribution is displayed as: number of conformations with respective torsional angle orientation/total number (i.e., nine) of conformations. ¥Conformation distribution is displayed as: number of conformations with respective torsional angle orientation/total number of conformations (A = 4, B = 8, C = 6 conformations).

Torsional Angle	Conformation Distribution of Optimized Carvedilol Low Energy Conformers (c.f. Table 12)‡			Conformation Distribution of Low Energy Carvedilol Fragments¥			
	g+	*a*	*g-*		*g+*	*a*	*g-*
χ_1	**8/9 (89%)**	1/9 (11%)	(0%)		**(0%)**	3/4 (75%)	1/4 (25%)
χ_2	(0%)	**9/9 (100%)**	(0%)	A	(0%)	**3/4 (75%)**	1/4 (25%)
χ_3	(0%)	(0%)	**9/9 (100%)**		(0%)	3/4 (75%)	**1/4 (25%)**
χ_4	**9/9 (100%)**	(0%)	(0%)		**3/8 (37.5%)**	5/8 (62.5%)	(0%)
χ_5	4/9 (44.4%)	**5/9 (55.6%)**	(0%)	B	2/8 (25%)	**6/8 (75%)**	(0%)
χ_6	3/9 (33.3%)	3/9 (33.3%)	3/9 (33.3%)		3/8 (37.5%)	3/8 (37.5%)	2/8 (25%)
χ_7	4/9 (44.4%)	(0%)	**5/9 (55.6%)**		3/6 (50%)	(0%)	**3/6 (50%)**
χ_8	2/9 (22.2%)	**5/9 (55.6%)**	2/9 (22.2%)	C	2/6 (33.3%)	**2/6 (33.3%)**	2/6 (33.3%)
χ_9	4/9 (44.4%)	(0%)	**5/9 (55.6%)**		3/6 (50%)	(0%)	**3/6 (50%)**
χ_{10}	**9/9 (100%)**	(0%)	(0%)	**A**	**3/4 (75%)**	(0%)	1/4 (25%) F.A.
				B	**8/8 (100%)**	(0%)	(0%)
				C	NA	NA	NA
χ_{11}	3/9 (33.3%)	**4/9 (44.4%)**	2/9 (22.2%)	**C**	2/6 (33.3%)	**2/6 (33.3%)**	2/6 (33.3%)

From **Table 16**, it is evident that the conformation distribution of eight (χ_2, χ_5, χ_6, χ_7, χ_8, χ_9, χ_{10}, and χ_{11}) of the 11 torsional angles were accurately predicted (72.7%). Given this assessment, one can deem the accuracy of this method as satisfactory. Inability to predict torsional angles χ_1, χ_3, and χ_4 is related to the fact that these were essentially rigid at one orientation for all low energy conformations pertaining to the tetra-centric structural motif. It is postulated that the inability to predict these torsional angles arises from the fact that Fragment A only has a terminal methyl group for χ_4 and not the secondary amine, and therefore, the complexity of this fragment was underestimated. Even so, the accuracy of this method is adequate because the inability to predict some conformational distributions was compensated by a high degree of prediction in other torsional angles such as χ_2, χ_5, χ_7, χ_9, and χ_{10} (c.f. **Table 16**).

With regards to utility and expediency, the current fragmentation method has greatly aided the problem of deciphering the low energy conformations of carvedilol. The robustness of this methodological approach has allowed the conversion of carvedilol's exhaustive PEHS into a series of smaller, well-defined, and more manageable conformational surfaces, while retaining major properties of the whole system. Although this method has obvious short-comings, it achieves its overall objectives while minimizing computational and experimental resources.

As theoretical and computational methods move progressively into the realm of larger molecular systems, there is a need to find ever-evolving methods, rather than relying on brute computing force, to effectively evaluate such complicated systems[59]. It has been previously postulated that, the success of such novel methodological approaches to finding the dominant conformations of large PEHSs *via* sampling, will be the ability of these methods to generate starting points (on parts of a PEHS) with some amount of energy minimization[59]. This will allow investigators to efficiently realize which parts of a PEHS they should focus on. The rational molecular fragmentation approach achieves this goal because the carvedilol map is not sampled randomly. Alternatively, the carvedilol fragments are optimized to generate inputs (i.e., from low energy optimized fragment conformations) with an inherent amount of energy minimization/optimization. This methodological standpoint greatly simplifies sampling a large PEHS like that of carvedilol's because it is oriented to hypothesized low energy conformers. A general diagrammatical outline of this fragmentation method is presented in **Figure 22**.

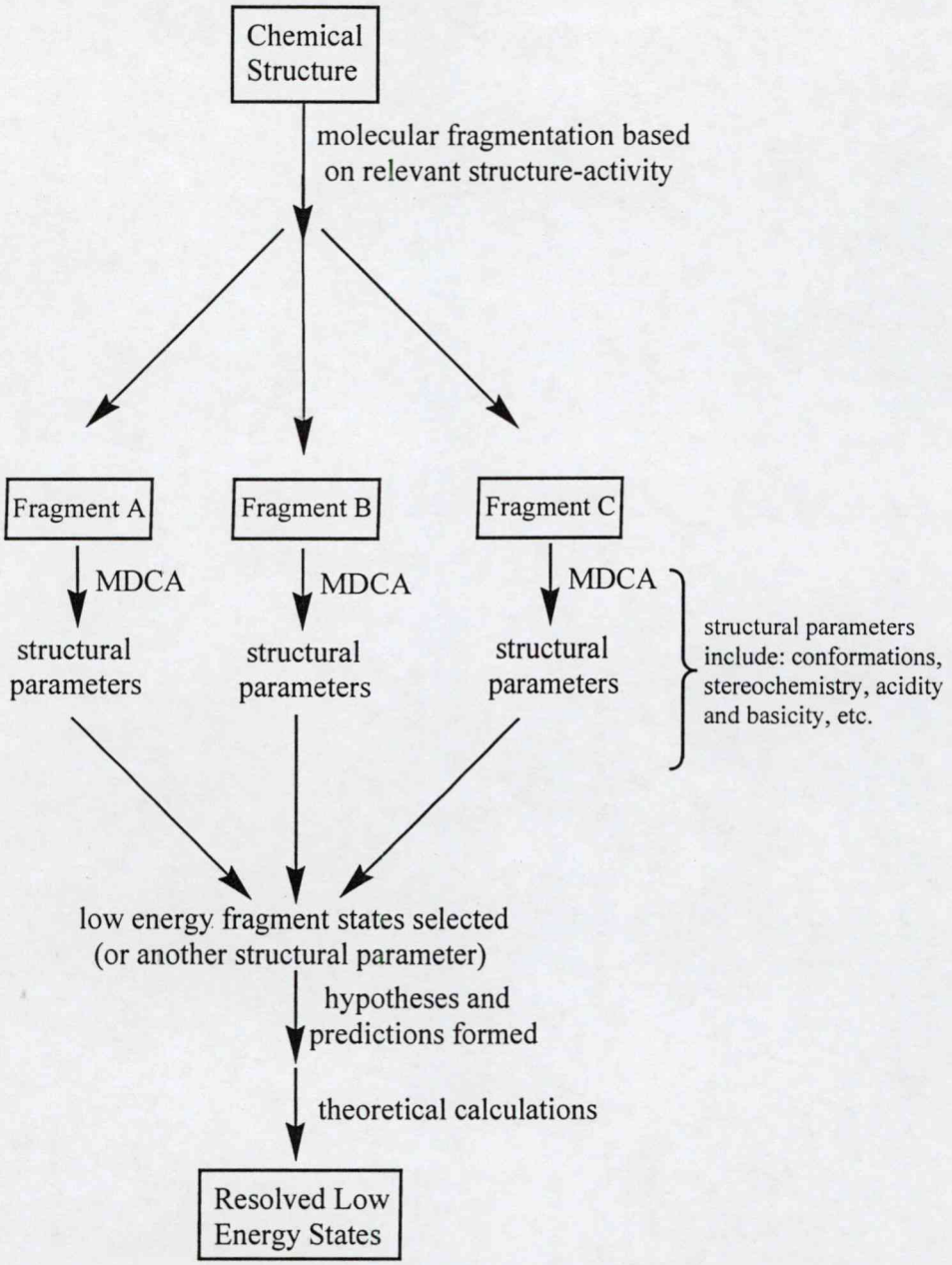

Figure 22: Diagrammatical representation of the rational molecular fragmentation method applied for the structural analysis of complex molecular systems. Note that, as shown for the carvedilol case study, conformations, as well as other structural parameters (stereochemistry, basicity, H-bonding, etc.), may be analyzed, predicted, optimized, resolved, and extrapolated with this approach to structural analysis.

6. CONCLUSIONS

6.1 MDCA of Carvedilol Fragments

Hartree-Fock [RHF/3-21G, RHF/6-31G(d)] and DFT [B3LYP/6-31G(d)] conformational analysis of the *R*- and *S*-4-(2-hydroxypropoxy)carbazol (Fragment A) PEHS revealed a total of 19 converged minima for each stereoisomer and four low energy (defined as possessing a conformer relative energy of less than two Kcal•mol^{-1}) conformers (*R*-Fragment A: *aaag+*, *aag-g-*, *ag-ag+*, *g-aag+*). Conformer stability was influenced by intramolecular H-bonding between the carbazole ether oxygen and hydroxyl proton. Hartree-Fock (RHF/3-21G) MDCA of 2(*S*)-1-(ethylamonium)propane-2-ol (Fragment B) converged 18 minima with eight conformers being deemed low energy states (*S*-Fragment B: *aaag+*, *ag+ag+*, *aag-g+*, *g+aag+*, *aag+g+*, *ag+g+g+*, *g+ag+g+*, *g+ag-g+*). All minima were dominated by a *gauche* plus effect in the rotation about carvedilol's C-OH bond at the Fragment B stereocentre (torsional angle χ_{10}). The carvedilol fragment, aminoethoxy-2-methoxy-benzene (Fragment C) was subject to geometry optimizations of its protonated PEHS. MDCA exposed a total of 24 converged minima; six low energy structures were isolated (Fragment C: *g+g+g+g-*, *g-g-g-g+*, *g+ag-a*, *g-ag+a*, *g+g-g-g+*, *g-g+g+g-*). Conformers with the lowest relative energies possessed a motif consisting of bifurcated H-bonds forming an eight-membered ring.

6.2 Stereochemical Parameters of Carvedilol Fragments & Carvedilol

The carbazole-containing fragment of carvedilol, *R*- and *S*-Fragment A, along with selected pro-chiral and chiral analogues, were subject to MDCA at the RHF/3-21G, RHF/6-31G(d), and B3LYP/6-31G(d) levels of theory to divulge the chiral parameters of carvedilol. Conformational analysis revealed the intrinsic energetic profiles associated with point chirality and axis chirality present in these structures. It is shown that axis chirality induced by an asymmetric distribution of electron density (generally as a result of asymmetric conformations) is a feature of all structures, and thus, does not require a point chiral centre. Further, both axis and point chiral-dependence can be exploited to predict properties of corresponding stereoisomeric pairs. Axis chirality was also confirmed for the Fragment C PEHS and point and axis chirality extrapolated for Fragment B and carvedilol.

6.3 Conformational-Dependence of Multiple Proton Basicity

After Hartree-Fock (RHF/3-21G) MDCA of their respective PEHSs, the secondary amine Fragment B and the primary amine Fragment C were independently deprotonated to disclose the effects of conformation on multiple proton basicity. The data presented for Fragment B and C substantially agree and support a direct dependence of multiple proton basicity on conformation as protons involved in IMAF will require a greater investment of energy for deprotonation. Hence, for carvedilol, and with respect to general protonophoretic pathways involving primary and secondary amines, reactions and events of deprotonation will not only favor higher energy conformations but will also favor protons differentially according to their orientation. It may be expected that the abstracted proton will be oriented maximally away from the core of the structure devoid of any IMAF for favoured energetics.

The data presented in this dissertation is evidence that, it is not the proton *per se* that determines whether energies of deprotonation are large or small; rather, it is the molecular conformation adopted by a structure that determines the respective orientation of a given proton, and therefore, predetermines the energetics of the deprotonation event. This is to say that, protons may be indistinguishable one from the other, but depending on the molecular conformations and the protonophoretic mechanisms in question, rarely are two protons the same. Thus, conformation will supercede and dictate the energetic basis of protonophoretic pathways and mechanisms.

6.4 Electronic Structure Prediction & Analysis of Carvedilol

6.4.1 Conformational Prediction of the Low Energy States of Carvedilol

Utilizing the structures and conformational assignments of respective low energy carvedilol fragments, a set of gas phase low energy carvedilol conformations were presented and evaluated. A total of 240 carvedilol conformers were initially optimized at the RHF/3-21G level of theory revealing 121 converged structures. An authentic set of nine converged low energy conformations were discovered for further examination.

6.4.2 DFT & NMR Structural Analysis of Carvedilol Conformers

The nine low energy structures of carvedilol optimized at Hartree-Fock were subject to high level DFT calculations in gas and solvent (DMSO and water). Independent NMR spectroscopy (in DMSO) was performed for further account of the focal carvedilol states. The DFT optimizations and NMR spectroscopy described in this dissertation consist of the most detailed account of the electronic structure and significant conformational intricacies of carvedilol available in the literature. Gas phase results show that seven of the nine conformers possess a novel tetra-centric spiro-type conformation composed of intramolecular six- and eight-membered rings. This structural motif is dictated by the necessary stabilization of the positive nitrogen centre and by the inflexibility of the carbazole aromatic ring. DMSO and water DFT optimizations and NMR spectroscopy closely mirror each other indicating that carvedilol has a subtle energetic and structural solvent effect and a significant barrier to re-arrangement from gas phase to solvent exists. ROESY, NOESY, and scalar J-coupling NMR spectra show further evidence of the rigid rotation about the large carbazole pharmacophore. Given the harmony achieved between theoretical and experimental results, this study suggests the most populated states of carvedilol expected to dominate physical and biological samples and it is expected that this will critically aid the molecular understating of carvedilol's pharmacodynamic mechanisms and structural underpinnings.

6.5 Rational Molecular Fragmentation of Carvedilol

Although carvedilol possesses an exorbitant amount of conformational possibilities, by utilizing a fragmentation approach based on the basic thermodynamics precept that only low energy states are significantly occupied, the highly populated states of carvedilol have been resolved. The *rational molecular fragmentation* method applied to carvedilol relies not on profligate computing force, but rather on the study of rationally-constructed fragments to divulge properties of the whole system as a means to generate PEHS points with some amount of energy minimization. The approach simplifies PEHS sampling because it is focused on conformers hypothesized to be highly populated states.

7. REFERENCES

1. J. Cheng, K. Kamiya, I. Kodama; Cardiovasc. Drug Rev. 19 (2001) 152.
2. W. Carlson, K. Oberg; J. Cardiovasc. Pharmacol. Ther. 4 (1999) 205.
3. S. Capomolla, O. Febo, M. Gnemmi, G. Riccardi, C. Opasich, A. Carporotondi, A. Mortara, G. Pinna, F. Cobelli; Am. Heart J. 139 (2000) 596.
4. D. McTavish, D. Campoli-Richards, E.M. Sorkin; Drugs 45 (1993) 232.
5. M. Packer, M.R. Bristow, J.N. Cohn, W.S. Colucci, M.B. Fowler, E.M. Gilbert, N.H. Shusterman (for The U.S. Carvedilol Heart Failure Study Group); N. Engl. J. Med. 334 (1996) 1349.
6. U. Hauf-Zachariou, R.A. Blackwood, K.A. Gunawardena, J.G. O'Donnell, S. Garnham, E. Pfarr; Eur. J. Clin. Pharmacol. 52 (1997) 95.
7. N. Noguchi, K. Nishino, E. Niki; Biochem. Pharmacol. 159 (2000) 1069.
8. T.L. Yue, P.G. Lysko, F.C. Barone, J.L. Gu, R.R. Ruffolo Jr., G.Z. Feuerstein; Ann. N.Y. Acad. Sci. 738 (1994) 230.
9. M. Guazzi, P. Agostoni, M. Matturri, G. Pontone, M.D. Guazzi; Am. Heart. J. 138 (1999) 460.
10. R.R. Ruffollo Jr., G.Z. Feuerstein; J. Cardiovasc. Pharmacol. 32 Suppl. 1 (1998) S22.
11. P.J. Oliveira, M.P. Marques, L.A.E. Batista de Carvalho, A.J.M. Moreno; Biochem. Biophys. Res. Commun. 276 (2000) 82.
12. J. Cheng, R. Niwa, K. Kamiya, J. Toyama, I. Kodama; Eur. J. Pharmacol. 376 (1999) 189.
13. R.A. Kelly, J.-L. Balligand, T.W. Smith; Circ. Res. 79 (1996) 363.
14. T. Masaki, M. Yanagisawa, K. Goto; Med. Res. Rev. 12 (1992) 391.
15. D.R. Howlett, A.R. George, D.E. Owen, R.V. Ward, R.E. Markwell; Biochem. J. 343 (1999) 419.
16. G.M. Keating, B. Jarvis; Drugs 63 (2003) 1697.
17. M.A. Berg, G.A. Chasse, E. Deretey, A.K. Fuzery, B.M. Fung, D.Y.K. Fung, H. Henry-Riyad, A.C. Lin, M.L. Mak, A. Mantas, M. Patel, I.V. Repyakh, M. Staikova, S.J. Salpietro, T.-H. Tang, J.C. Vank, A. Perczel, G.I. Csonka, O. Farkas, L.L. Torday, Z. Szekely, I.G. Csizmadia; J. Mol. Struct. (THEOCHEM) 500 (2000) 5.
18. A. Coats; Hosp. Med. 64 (2003) 288.
19. R.H. Arnold, E. Kotlyar, C. Hayward, A.M. Keogh, P.S. Macdonald; Heart 89 (2003) 293.
20. M.C. Gerson, L.L. Craft, N. McGuire, D.P. Suresh, W.T. Abraham, L.E. Wagoner; J. Nucl. Cardiol. 9 (2002) 608.
21. L. Klein, C.M. O'Connor, W.A. Gattis, M. Zampino, L. de Luca, A. Vitarelli, F. Fedele, M. Gheorghiade; Am J Cardiol 91 (2003) 18F.
22. W. Bartsch, G. Sponer, K. Strein, B. Muller-Beckmann, L. Kling, E. Bohm, U. Martin, H.O. Borbe; Eur. J. Clin. Pharmacol. 38 Suppl. 2 (1990) S104.
23. R.R. Ruffolo Jr., G.Z. Feuerstein; Cardiovasc. Drugs Ther. 11 (1997) 247.
24. G. Feuerstein, N.H. Shusterman, R.R. Ruffolo Jr.; Drugs Today 33 (1997) 453.
25. G. Feuerstein, T.L. Yue, X. Ma, R.R. Ruffolo; Prog. Cardiovasc. Dis. 41 Suppl. 1 (1998) 17.
26. N. Noguchi, K. Nishino, E. Niki; Biochem. Pharmacol. 59 (2000) 1069.
27. B. Tadolini, F. Franconi; Free Radic. Res. 29 (1998) 377.
28. T.L. Yue, H.-Y. Cheng, P.G. Lysko; J. Pharmacol. Exp. Ther. 263 (1992) 92.

29. P. Dandona, R. Karne, H. Ghanim, W. Hamouda, A. Aljada, C.H. Magsino; Circulation 101 (2000) 122.
30. R. Feurestein, T.-L. Yue; Pharmacology 48 (1994) 385.
31. T.L. Yue, P.J. Mckenna, P.G. Lysko, J.L. Gu, K.A. Lysko, R.R. Ruffolo Jr., G.Z. Feuerstein; Eur. J. Pharmacol. 251 (1994) 237.
32. S. Jacob, K. Rett, M. Wicklmayr, B. Agrawal, H.J. Augustin, G.J. Dietze; J. Hypertens. 14 (1996) 489.
33. D. Giugliano, R. Acampora, R. Marfella, N. De Rosa, P. Ziccardi, R. Ragone, L. De Angelis, F. D'Onofrio; Ann. Intern. Med. 126 (1997) 955.
34. S. Jacob, K. rett, E.J. Henriksen; Am. J. Hypertens. 11 (1998) 1258.
35. Amiodarone Trials Meta-Analysis Investigators; Lancet 350 (1997) 1417.
36. C.-P. Sung, A.J. Arleth, E.H. Ohlstein; J. Cardiovasc. Pharmacol 21 (1993) 221.
37. E.H. Ohlstein, S.A. Douglas, C.P. Sung, T. Yue, C. Louden, A. Arleth, G. Poste, R.R. Ruffolo Jr., G.Z. Feuerstein; Proc. Natl. Acad. Sci. USA 90 (1993) 6189.
38. N. Khandoudi, J. Percevault-Albadine, A. Bril; J. Cardiovasc. Pharmacol. 32 (1998) 443.
39. G. Feuerstein, G.-L. Liu, T.L. Yue, H.-Y. Cheng, J.P. Hieble, J.R.S. Arch, R.R. Ruffolo, X.-L. Ma; Eur. J. Pharmacol. 351 (1998) 341.
40. E.H. Ohlstein, L. Vickery, A. Arleth, F. Barone, C.P. Sung, A. Camden, L. McCartney; Clin. Exp. Hypertens. 16 (1994) 163.
41. F.C. Barone, W.G. Campbell Jr., A.H. Nelson, G.Z. Feuerstein; J. Hypertens. 16 (1998) 871.
42. P.E. Massart, J. Donckier, J. Kyselovic, T. Godfraind, G.R. Heyndrickx, M. Wibo; Hypertension 34 (1999) 1197.
43. A. Bril, V. Tomasi, M.-P. Laville; Pharmacol. Commum. 5 (1995) 281.
44. H. Brunvand, L. Frlyland, E. Hexeberg, S.E. Rynning, R.K. Berge, K. Grong; Eur. J. Pharmacol. 314 (1996) 99.
45. Y.T. Sia, T.G. Parker, J.N. Tsoporis, P. Liu, A. Adam, J.L. Rouleau; J. Cardiovasc. Pharmacol. 39 (2002) 73.
46. P.G. Heytler, 1979, Uncouplers of Oxidative Phosphorylation. In Methods in Enzymology, LV, Academic Press Inc., New York, pp. 462-472.
47. A. Tzagoloff, 1982. Mitochondria, Plenum Press, New York.
48. S.S. Korshunov, V.P. Skulachev, A.A. Starkov; FEBS Lett 416 (1997) 15.
49. J. Hardy, J. Selkoe; Science 297 (2002) 353.
50. V.M.-Y. Lee; Neurobiol. Aging 23 (2002) 1039.
51. D.M. Walsh, I. Klyubin, J.V. Fadeeva, W.K. Cullen, R. Anwyl, M.S. Wolfe, M.J. Rowan, D.J. Selkoe; Nature 416 (2002) 535.
52. M.P. Lambert, A.K. Barlow, B.A. Chromy, C. Edwards, R. Freed, M. Liosatos, T.E. Morgan, I. Rozovsky, B. Trommer, K.L. Viola, P. Wals, C. Zhang, C.E. Finch, G.A. Krafft, W.L. Klein; Proc. Natl. Acad. Sci. USA 95 (1998) 6448.
53. D.M. Walsh, D.M. Hartley, Y. Kusumoto, Y. Fezoui, M.M. Condron, A. Lomakin, G.B. Benedek, D.J. Selkoe, D.B. Teplow; J. Biol. Chem. 274 (1999) 25945.
54. D.-H. Chui, H. Tanahashi, K. Ozawa, S. Ikeda, F. Checler, O. Ueda, H. Suzuki, W. Araki, H. Inoue, K. Shirotani, K. Takahashi, F. Gallyas, T. Tabira; Nature Med. 5 (1999) 560.
55. R.R. Ruffolo Jr., M. Gellai, J.P. Hieble, R.N. Willette, A.J. Nichols; Eur. J. Clin. Pharmacol. 38 (1990) S82.

56. F.A. Carroll. In Perspectives on Structure and Mechanism in Organic Chemistry; Brooks/Cole Publishing Company; Pacific Grove, California, 1998; pp. 78-80.
57. H. Hirschmann, K.R. Hanson; Top. Stereochem. 14 (1983) 183.
58. W.C. Agosta; J. Am. Chem. Soc. 86 (1964) 2638.
59. E. Billings. Molecular Modeling and Drug Design. In Foye's Principles of Medicinal Chemistry, 5th ed.; Williams, D.A., Lemke, T.L., Eds.; Lippincott Williams & Wilkins: New York, 2002; pp 68-85.
60. W.-M. Chen, L.-M. Zeng, K.-B. Yu, J.-H. Xu; Chinese J. Struct. Chem. 17 (1998) 325.
61. Gaussian 98 (Revision A.9), M.J. Frisch, G.W. Trucks, H.B. Schlegel, G.E. Scuseria, M.A. Robb, J.R. Cheeseman, V.G. Zakrzewski, J.A. Montgomery, Jr., R.E. Stratmann, J.C. Burant, S. Dapprich, J.M. Millam, A.D. Daniels, K.N. Kudin, M. C. Strain, O. Farkas, J. Tomasi, V. Barone, M. Cossi, R. Cammi, B. Mennucci, C. Pomelli, C. Adamo, S. Clifford, J. Ochterski, G.A. Petersson, P. Y. Ayala, Q. Cui, K. Morokuma, D.K. Malick, A.D. Rabuck, K. Raghavachari, J.B. Foresman, J. Cioslowski, J.V. Ortiz, A.G. Baboul, B.B. Stefanov, G. Liu, A. Liashenko, P. Piskorz, I. Komaromi, R. Gomperts, R.L. Martin, D.J. Fox, T. Keith, M.A. Al-Laham, C.Y. Peng, A. Nanayakkara, C. Gonzalez, M. Challacombe, P.M.W. Gill, B.G. Johnson, W. Chen, M.W. Wong, J.L. Andres, M. Head-Gordon, E.S. Replogle and J.A. Pople, Gaussian, Inc., Pittsburgh PA, 1998.
62. A.D. Becke; J. Chem. Phys. 98 (1993) 5648.
63. Axum 5.0C for Windows, MathSoft Incorporated, 1996.
64. Excel for Windows, Microsoft, 2002.
65. M.W. Wong, M.J. Frisch, K.B. Wiberg; J. Am. Chem. Soc. 113 (1991) 4776.
66. M.W. Wong, K.B. Wiberg, M.J. Frisch; J. Am. Chem. Soc. 114 (1992) 523.
67. M.W. Wong, K.B. Wiberg, M.J. Frisch; J. Chem. Phys. 95 (1991) 8991.
68. M.W. Wong, K.B. Wiberg, M.J. Frisch; J. Am. Chem. Soc. 114 (1992) 1645.
69. J.G. Kirkwood; J. Chem. Phys. 2 (1934) 351.
70. L. Onsager; J. Am. Chem. Soc. 58 (1936) 1486.
71. J.B. Foresman, A. Frish. 1996, Reaction field models of solvation. In Exploring Chemistry with Electronic Structure Methods, 2nd edition, Gaussian Inc., Pittsburgh, pp. 237-249.
72. J.C.P. Koo, J.S.W. Lam, G.A. Chass, L.L. Torday, A. Varro, J.Gy. Papp; J. Mol. Str. (THEOCHEM) 620 (2003) 231.
73. W.H. Schaeffer, J. Politowski, B. Hwang, F. Dixon Jr., A. Goalwin, L. Gutzait, K. Anderson, C. Debrosse, M. Bean, G.R. Rhodes; Drug Metab Dispos 26 (1998) 958.

8. APPENDIX A

This dissertation is based on the following papers now published or accepted or submitted.

1. **David R. P. Almeida**, Luca F. Pisterzi, Gregory A. Chass, Ladislaus L. Torday, Andras Varro, Julius Gy. Papp, and Imre G. Csizmadia. A density functional molecular study on the full conformational space of the *S*-4-(2-hydroxy propoxy)carbazol fragment of carvedilol (1-(9H-Carbazol-4-yloxy)-3-[2-(2-methoxy-phenoxy)ethylamino]-2-propanol) in vacuum and in different solvent media, J. Phys. Chem. A, 106 (2002), 10423-10436.

2. **David R. P. Almeida**, Donna M. Gasparro, Luca F. Pisterzi, Ladislaus L. Torday, Andras Varro, Julius Gy. Papp, and Botond Penke. Gas phase conformational basicity of carvedilol Fragment B, 2(S)-1-(ethylamonium)propane-2-ol: An ab initio study on a protonophoretic of oxidative phosphorylation uncoupling, J. Mol. Str. (THEOCHEM), 631 (2003), 251-270.

3. **David R. P. Almeida**, Donna M. Gasparro, Luca F. Pisterzi, Ladislaus L. Torday, Andras Varro, Julius Gy. Papp, Botond Penke, and Imre G. Csizmadia. Molecular study on the enantiomeric relationships of carvedilol Fragment A, 4-(2-hydroxypropoxy)carbazol, along with selected analogues, J. Phys. Chem. A, 107 (2003), 5594-5610.

4. **David R. P. Almeida**, Donna M. Gasparro, Luca F. Pisterzi, Jason R. Juhasz, Ferenc Fülöp, and Imre G. Csizmadia. Conformational-dependent basicity of carvedilol Fragment C: An ab initio study on the primary amine, aminoethoxy-2-methoxy-benzene, J. Mol. Str. (THEOCHEM), 666-667 (2003), 557-580.

5. **David R. P. Almeida**, Donna M. Gasparro, Luca F. Pisterzi, Jason R. Juhasz, Ferenc Fülöp, and Imre G. Csizmadia. Predicting the conformations of carvedilol based on its pharmacophore fragments: A gas phase and solvation ab initio and density functional study, J. Mol. Str. (THEOCHEM), 666-667 (2003), 537-545.

6. **David R. P. Almeida**, Donna M. Gasparro, Ferenc Fülöp, and Imre G. Csizmadia. Pharmacophore fragment-based prediction and gas phase ab initio optimization of carvedilol conformations, J. Phys. Chem. A, (2004), in press.

7. **David R. P. Almeida**, Donna M. Gasparro, Tamas A. Martinek, Ferenc Fülöp, and Imre G. Csizmadia. Resolution of carvedilol's conformational surface via gas and solvent phase density functional theory optimizations and NMR spectroscopy, J. Phys. Chem. A, submitted for publication (2004).